Article

Cell Reports

Protein Prenylation Constitutes an Endogenous Brake on Axonal Growth

Graphical Abstract

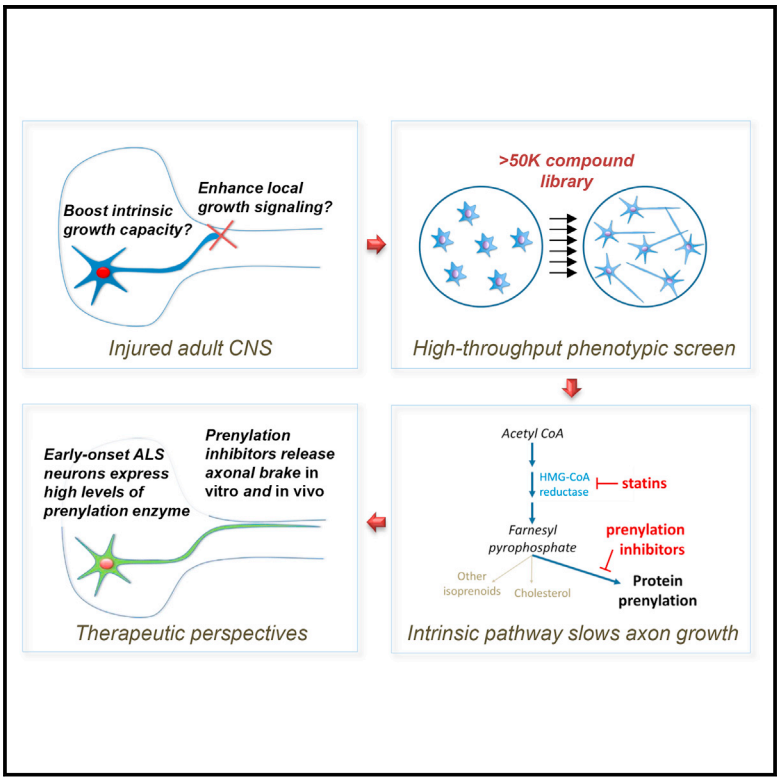

Highlights

- Statins are the most potent enhancers of neurite elongation in vitro
- Statins and protein prenylation inhibitors promote CNS axon regeneration in vivo
- Motor neurons of early-onset ALS patients express high levels of prenylation enzyme
- Prenylation inhibitors provide a potential therapeutic approach for CNS regeneration

Authors

Hai Li, Takaaki Kuwajima, Derek Oakley, ..., Marie T. Filbin, Brent Stockwell, Christopher E. Henderson

Correspondence

chris.henderson@biogen.com

In Brief

Using a high-throughput phenotypic screen, Li et al. identify statins and inhibitors of protein prenylation as potent neurite-outgrowth-promoting agents. High levels of prenylation enzyme are found in patients with earlier-onset forms of ALS. Prenylation may limit axonal growth in both normal and pathological situations.

Li et al., 2016, Cell Reports *16*, 545–558
July 12, 2016 © 2016
http://dx.doi.org/10.1016/j.celrep.2016.06.013

Cell Reports
Article

Protein Prenylation Constitutes an Endogenous Brake on Axonal Growth

Hai Li,[1,3] Takaaki Kuwajima,[1,3] Derek Oakley,[6,11] Elena Nikulina,[4] Jianwei Hou,[4] Wan Seok Yang,[1,5,12] Emily Rhodes Lowry,[6] Nuno Jorge Lamas,[3,6,7] Mackenzie Weygandt Amoroso,[6,13] Gist F. Croft,[6,14] Raghavendra Hosur,[9] Hynek Wichterle,[1,3,6] Said Sebti,[8] Marie T. Filbin,[4] Brent Stockwell,[1,5] and Christopher E. Henderson[1,2,3,6,10,15,*]

[1]Center for Motor Neuron Biology and Disease, Columbia Stem Cell Initiative, Columbia Translational Neuroscience Initiative, Columbia University, New York, NY 10032, USA
[2]Department of Rehabilitation and Regenerative Medicine
[3]Department of Pathology and Cell Biology, Neurology, and Neuroscience College of Physicians and Surgeons, Columbia University, New York, NY 10032, USA
[4]Department of Biological Sciences, Hunter College, City University of New York, NY 10065, USA
[5]Howard Hughes Medical Institute and Department of Biological Sciences and Department of Chemistry, Columbia University, New York, NY 10027, USA
[6]Project A.L.S./Jenifer Estess Laboratory for Stem Cell Research, New York, NY 10032, USA
[7]Life and Health Sciences Research Institute, School of Health Sciences, University of Minho, 4710-057 Braga, Minho, Portugal
[8]Moffitt Cancer Center and Research Institute, University of South Florida, Tampa, FL 33612, USA
[9]Computational Biology, Biogen Inc., Cambridge, MA 02142, USA
[10]Target ALS Foundation, New York, NY 10032, USA
[11]Present address: Department of Pathology, Massachusetts General Hospital, Boston, MA 02114, USA
[12]Present address: Department of Biological Science, St. John's University, Jamaica, NY 11439, USA
[13]Present address: Center for Brain Science, Harvard University, Cambridge, MA 02138, USA
[14]Present address: Laboratory of Stem Cell Biology and Molecular Embryology, Rockefeller University, New York, NY 100665, USA
[15]Present address: Neurology Research, Biogen, Inc., Cambridge, MA 02142, USA
*Correspondence: chris.henderson@biogen.com
http://dx.doi.org/10.1016/j.celrep.2016.06.013

SUMMARY

Suboptimal axonal regeneration contributes to the consequences of nervous system trauma and neurodegenerative disease, but the intrinsic mechanisms that regulate axon growth remain unclear. We screened 50,400 small molecules for their ability to promote axon outgrowth on inhibitory substrata. The most potent hits were the statins, which stimulated growth of all mouse- and human-patient-derived neurons tested, both in vitro and in vivo, as did combined inhibition of the protein prenylation enzymes farnesyltransferase (PFT) and geranylgeranyl transferase I (PGGT-1). Compensatory sprouting of motor axons may delay clinical onset of amyotrophic lateral sclerosis (ALS). Accordingly, elevated levels of *PGGT1B*, which would be predicted to reduce sprouting, were found in motor neurons of early- versus late-onset ALS patients postmortem. The mevalonate-prenylation pathway therefore constitutes an endogenous brake on axonal growth, and its inhibition provides a potential therapeutic approach to accelerate neuronal regeneration in humans.

INTRODUCTION

Axonal growth is an essential step in the formation of neural circuits during normal development. In cases of traumatic brain injury or neurodegenerative disease, axonal damage is among the first morphological manifestations, and suboptimal regeneration is thought to be a major contributor to the low rates of functional recovery. Enhancing axonal regeneration in a controlled manner in patients with spinal cord injury may allow them to regain key lost functions; similar treatment in patients with amyotrophic lateral sclerosis (ALS) has the potential to increase muscle strength over the course of the disease. Over the past few decades, we have gained considerable insight into the extrinsic factors and intrinsic signaling mechanisms that affect directional choices taken by the axon growth cone and govern its reduced ability to advance in the damaged CNS (Alizadeh et al., 2015). However, we still have little knowledge of the cell-intrinsic mechanisms that drive axonal forward growth.

Over the past few decades, much insight has been gained into the low regenerative capacity of the adult CNS (Liu et al., 2011; Yiu and He, 2006). Most studies have focused on extrinsic factors that restrict axon regeneration (Filbin, 2003; Thiede-Stan and Schwab, 2015). Three growth inhibitors—myelin-associated glycoprotein (MAG), Nogo, and oligodendrocyte myelin glycoprotein—act through a common receptor complex containing the ligand-binding Nogo-66 receptor (NgR) and its

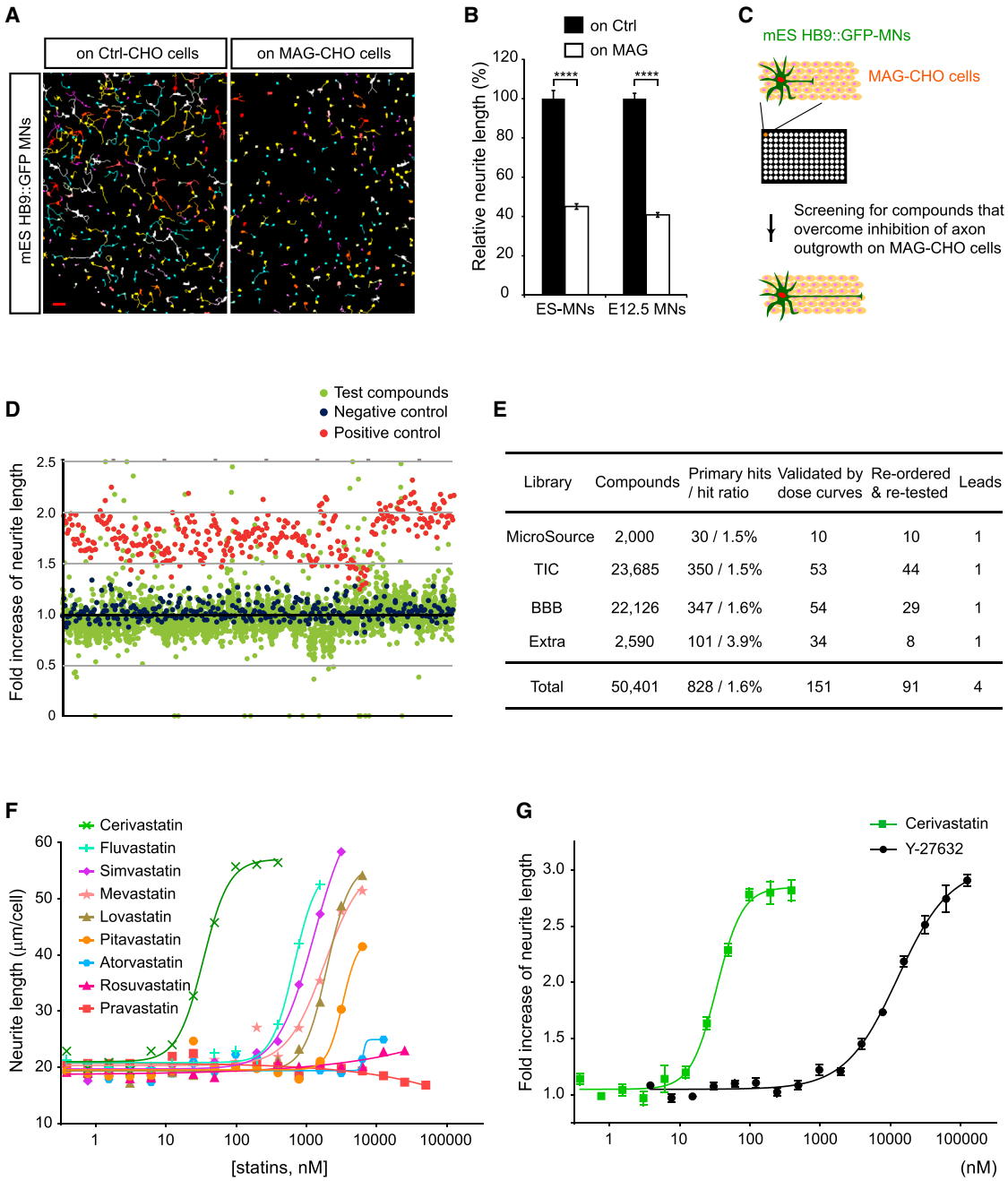

Library	Compounds	Primary hits / hit ratio	Validated by dose curves	Re-ordered & re-tested	Leads
MicroSource	2,000	30 / 1.5%	10	10	1
TIC	23,685	350 / 1.5%	53	44	1
BBB	22,126	347 / 1.6%	54	29	1
Extra	2,590	101 / 3.9%	34	8	1
Total	50,401	828 / 1.6%	151	91	4

Figure 1. High-Throughput Screen for Small Molecules that Enhance Neurite Outgrowth on Inhibitory Substrata Identifies Statins as the Most Potent Hits

(A) Fields of live mouse ES-MNs expressing the *Hb9::GFP* transgene imaged through monolayers of control CHO (Ctrl-CHO) or MAG-CHO cells. False colors are assigned to individual neurons by MetaMorph, which calculates neurite outgrowth parameters on a cell-by-cell basis. Neurite outgrowth on MAG-CHO cells is severely restricted, but cell survival is little affected. Scale bar, 100 μm.

(B) ES-MNs and E12.5 primary mouse motor neurons show comparable growth inhibition on MAG-CHO (mean ± SEM, n = 8; $p < 0.005$ for both ES-MNs and primary MNs).

(C) Schematic of the high-throughput screen.

(D) A snapshot of a fraction of the screening data. Neurite outgrowth data were converted to fold-increase by normalizing them to the negative controls in each plate. Data collected from forty 96-well plates are plotted for negative and positive controls, as well as test compounds.

(E) Compound libraries used for the screen. The number of compounds screened, primary hit rate, number of hits validated and number of confirmed lead compounds (>1.8-fold increase) are indicated.

(legend continued on next page)

signaling co-receptors $p75^{NTR}$ and paired immunoglobulin-like receptor B (PirB). Key components of the glial scar are the chondroitin sulfate proteoglycans (CSPGs), a family of extracellular matrix proteins that inhibit axon outgrowth (Dickendesher et al., 2012; Lang et al., 2014; Shen et al., 2009; Snow et al., 2003).

Preventing extrinsic inhibitory signals has real potential for promoting CNS axon regeneration (Case and Tessier-Lavigne, 2005). In addition, however, complementary approaches aiming to boost axonal growth without targeting a specific inhibitory mechanism also have potential therapeutic impact. Among small molecules reported to be active on axon growth are monastrol, an inhibitor of kinesin-5 (Baas and Matamoros, 2015), and inhibitors of the mevalonate pathway, through which cholesterol and isoprenoids are synthesized from acetyl-coenzyme A (Figure 3A; Pooler et al., 2006). However, the latter compounds were tested at high concentrations that have been found to be cytotoxic in other studies (Butterfield et al., 2011). Moreover, those small molecules that have been shown to be effective in the CNS in vivo, such as cyclic AMP (cAMP)/rolipram, ROCK inhibitor, and polyamines, lack the specificity and potency expected of clinical candidates (Fournier et al., 2003; Nikulina et al., 2004; Cai et al., 1999, 2002). There is therefore a need to explore more broadly ways in which the suboptimal intrinsic growth capacity of adult CNS neurons can be boosted.

Phenotypic cell-based screening provides a powerful, unbiased chemical genetic approach to identifying novel mechanisms underlying a given cellular process. Earlier studies taking this approach to axonal growth used relatively small screening libraries (<2,000 small molecules; Al-Ali et al., 2015; Koprivica et al., 2005; Ma et al., 2010; Usher et al., 2010). We instead developed a high-throughput screen using neurons grown in the presence of myelin inhibitors. The screen identified four active compound classes, of which we focused on the cholesterol-lowering drugs statins. We show that statins are the most potent agents reported to promote growth of mouse and human neurons in culture and show strong regenerative effects when administered to injured CNS neurons in vivo. Statin activity in this system entirely reflects downstream inhibition of protein prenylation, and specific inhibitors of this post-translational modification replicate all the key effects of statins without perturbing cholesterol metabolism. Strikingly, postmortem motor neurons from patients with early-onset ALS express abnormally high endogenous levels of mRNA for the prenylation enzyme geranylgeranyl transferase I, which our data would predict to reduce their capacity for compensatory sprouting at the neuromuscular junction. Taken together, our data identify prenylation as a common intrinsic regulator of axonal growth rate and point to novel therapeutic approaches for CNS injury and neurodegenerative disease.

RESULTS

High-Throughput Screening for Small Molecules that Promote Neurite Regeneration

To identify mechanisms of axonal regeneration, we developed a high-throughput neuron-based assay (Figure 1). We used rodent motor neurons, since drugs screened on primary rat motor neurons subsequently showed efficacy in the clinic (Bordet et al., 2007). For ease of scale-up, mouse embryonic stem cell-derived motor neurons (mES-MNs) expressing an Hb9::GFP reporter (~50% abundance) were employed (ESCs; Wichterle et al., 2002). To quantify neurite outgrowth with minimal sampling error, we used fluorescence live imaging of whole wells in 96-well format (typically 300–700 neurons imaged per well) followed by automated image analysis that identified individual neurons and calculated the neurite length for each (Figure 1A).

To mimic the inhibitory cellular environment of the adult CNS, ES-MNs were grown on monolayers of CHO cells expressing MAG (Mukhopadhyay et al., 1994). After 20 hr in culture, neurite outgrowth of ES-MNs on MAG-CHO cells was only 47% ± 2% (mean ± SEM, n = 8) of that on control CHO cells (Figures 1A and 1B), whereas neuronal survival was only slightly affected (MAG-CHO 92% ± 1% of control; $p < 0.008$). Primary embryonic day 12.5 (E12.5) mouse motor neurons showed the same degree of growth inhibition on MAG-CHO cells (Figure 1B). Increasing cAMP levels has been shown to overcome MAG inhibition of axonal growth (Qiu et al., 2002), and the phosphodiesterase inhibitor rolipram promotes regeneration in vivo (Nikulina et al., 2004). Accordingly, forskolin promoted neurite growth in our assay, with a half-maximal effective concentration (EC_{50}) of 0.85 ± 0.08 μM (Figure S1A), as did a combination of forskolin (10 μM) and IBMX (100 μM), which was used as a positive control for the screen (Figure S1B). Our assay therefore faithfully reproduced the activity of compounds known to enhance axonal regeneration in vivo.

We screened a library of 50,401 compounds at a single concentration (10 μM) for their ability to overcome MAG inhibition (Figure 1C; see Experimental Procedures for the compound collections tested and for assay optimization procedures). Approximately 98% of compounds showed no significant effect on neurite outgrowth, while a minority were toxic (Figures 1D and 1E). Initial hits were defined as compounds that increased neurite outgrowth by >30% (initial hit rate, 1.6%; Figure 1E). In repeat assays using five-point 2-fold dilution series, 151 compounds were confirmed to be active. Of these, 91 were reordered from vendors and tested in a nine-point 2-fold dilution series in six replicates. Finally, four compounds that enhanced neurite outgrowth by >80% at their optimal concentration(s) were selected as leads (Figure S1C). One was a hitherto undescribed compound with no identified target. The second lead shows 90% similarity to a class of phosphodiesterase 4 inhibitors (PDE4; Skoumbourdis et al., 2008) and likely acts by

(F) Dose-response curves for all nine statins on ES-MNs grown on MAG-CHO monolayers. Note that six out of nine statins enhance neurite outgrowth >2-fold over MAG after 20 hr in culture. Values are means of six replicates; error bars are not shown for clarity.
(G) Cerivastatin is nearly 400-fold more potent than the ROCK inhibitor Y-27632 (mean ± SEM; n = 6 wells; data are representative of three independent experiments).

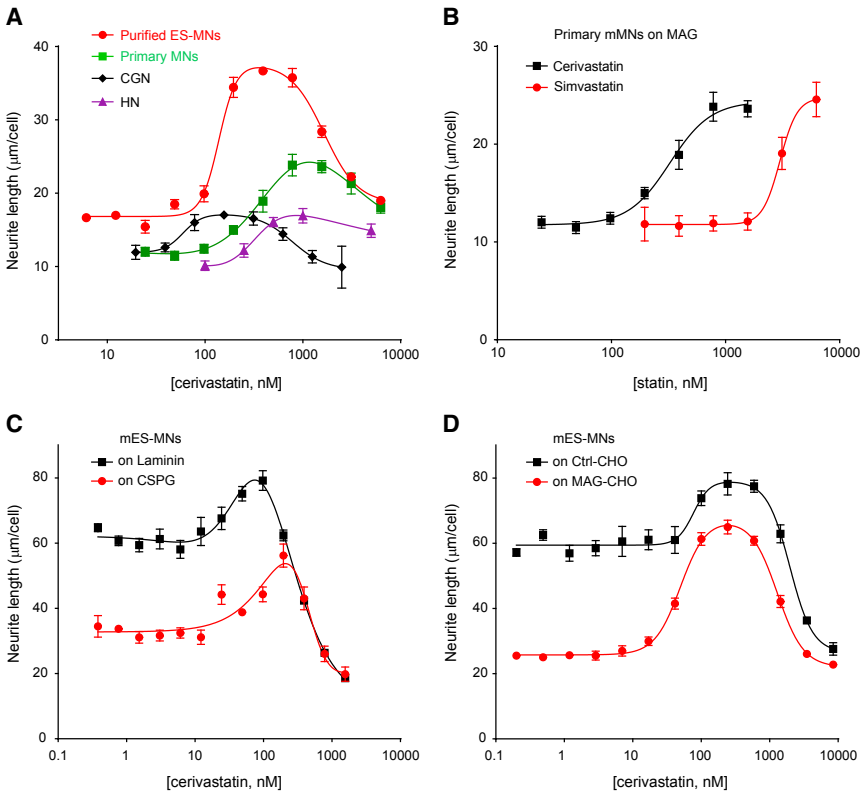

Figure 2. Statins Enhance Neurite Growth of Multiple Neuronal Classes on All Culture Substrata Tested

Effects of statins on neurite outgrowth were measured using different neuronal preparations cultured on both inhibitory and permissive substrata.

(A) Purified mouse ES-MNs, enriched mouse spinal motor neurons from E12.5 embryos (primary MNs), primary cerebellar granule neurons from postnatal day 2 (P2) to P6 mice (CGN), and primary hippocampal neurons from P1 rats (HN) grown on MAG-CHO monolayers all respond to cerivastatin in the sub-micromolar range.

(B) Primary (E12.5) motor neurons were grown on MAG-CHO monolayers in the presence of the indicated concentrations of cerivastatin and simvastatin. As with ES-MNs, the maximal effects are similar but cerivastatin is ~10-fold more potent.

(C) Growth of mouse ES-MNs is enhanced by cerivastatin on another inhibitory substratum (CSPG) and even in the most permissive culture conditions (polyornithine-laminin).

(D) Cerivastatin enhances growth on both CHO and MAG-CHO layers with a similar maximum level of outgrowth (C and D: mean ± SEM; n = 6; data are representative of at least three independent experiments).

increasing endogenous cAMP levels. The third lead (Figure S1C) bore a close resemblance to a family of kinesin-5 inhibitors, others of which have been reported to trigger axonal outgrowth in culture (Haque et al., 2004). Our open-ended screen was therefore able to detect modulators of known growth-inhibitory pathways. However, we detected no biological activity in this system for either of two small molecules reported to show neurite outgrowth-promoting properties: daidzein (Ma et al., 2010) or erlotinib (Koprivica et al., 2005; Figure S1D). Subsequently, therefore, we focused on the fourth and most potent lead, simvastatin.

Statins Act Directly on CNS Neurons to Promote Neurite Outgrowth on Multiple Substrata

Simvastatin is a widely used cholesterol-lowering drug. Six of the other commercially available drugs (cerivastatin, fluvastatin, simvastatin, lovastatin, mevastatin, and pitavastatin) enhanced ES-MN neurite outgrowth on MAG by >2-fold at concentrations ranging from 30 nM to 7 μM (Figure 1F). The remaining three (pravastatin, rosuvastatin, and atorvastatin) showed only weak activity, perhaps because they were designed to be selective for liver cells (Buckett et al., 2000; McTaggart et al., 2001). Cerivastatin was the most potent and induced a ~3-fold increase in neurite outgrowth with an EC_{50} of 33.6 ± 2.2 nM (mean ± SEM; n = 6), completely overcoming MAG inhibition (Figure 3B). Cerivastatin was 380-fold more potent in this system than the benchmark ROCK inhibitor Y-27632 (Figure 1G) (Fournier et al., 2003). We therefore used cerivastatin as a tool compound to study the mechanism of action of statins on neurite outgrowth.

To exclude the possibility that statins act indirectly through other cell types in the culture, we showed that MAG protein levels in MAG-CHO cells were not changed (Figures S2A and S2B) and that the effects of cerivastatin on fluorescence-activated cell sorting (FACS)-purified ES-MNs were similar to those on mixed cultures, increasing outgrowth 2.5-fold with an EC_{50} of 94.7 ± 6.9 nM (Figure 2A). Primary motor neurons from E12.5 ventral spinal cord from *Hb9::GFP* mice responded similarly to statins, though at slightly higher doses than for ES-MNs (Figures 2A and 2B). Lastly, both primary hippocampal (HN) and primary cerebellar granule neurons (CGN) respond to statins (Figure 2A). Thus, statins act directly on all neuronal populations tested.

To determine whether statins only inhibit a MAG-specific signaling mechanism (Filbin, 2003) or act more broadly on regeneration, we administered cerivastatin to ES-MNs grown on different substrata. Cerivastatin was also effective when CSPG was added to the culture medium (Figure 2C). Even on two permissive substrata, polyornithine-laminin and control CHO cells (which showed higher basal neurite outgrowth), we observed a significant increase in outgrowth (Figures 2C and 2D). Although cerivastatin has a significant effect on neurite initiation, its strongest dose-dependent effects are on axon elongation (Figures S2C–S2F). Therefore, statins act as potent general promoters of neurite outgrowth on all substrata tested, suggesting that basal levels of signaling through the mevalonate

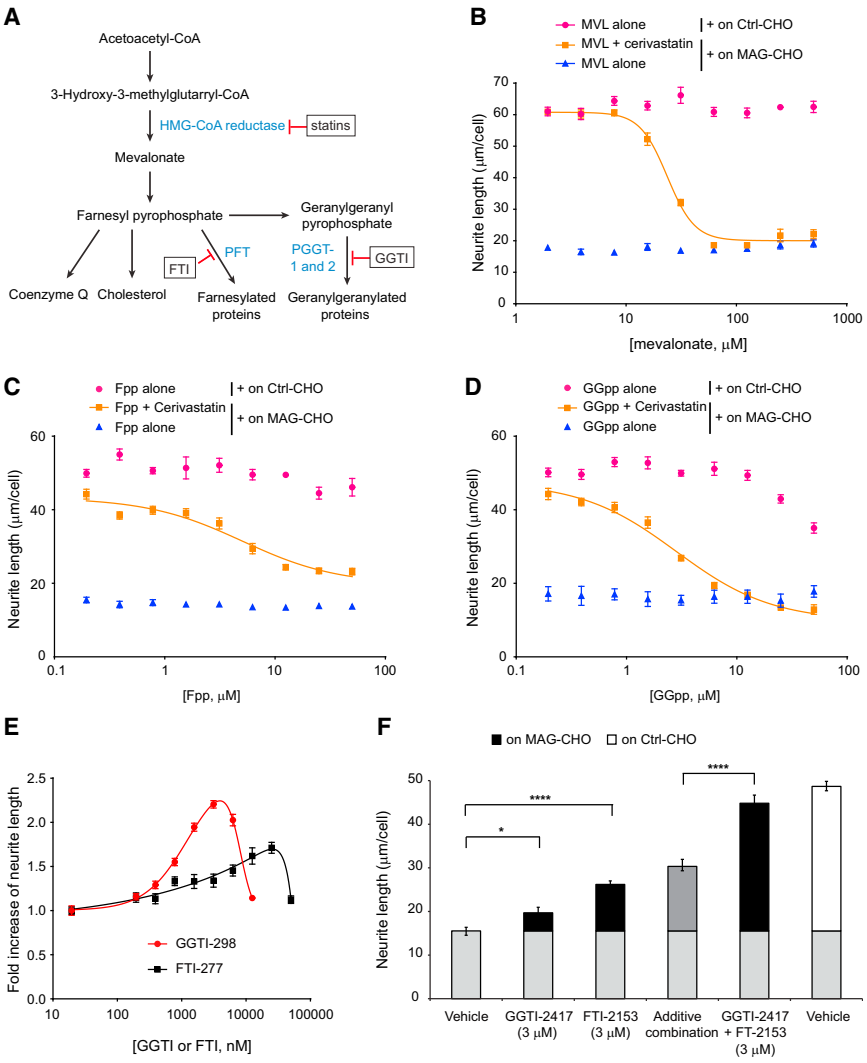

Figure 3. Statins Promote Neurite Growth by Inhibiting Both Prenylation Pathways

(A) Key intermediates in the mevalonate pathway leading to cholesterol and other isoprenoid biosynthesis as well as protein prenylation.

(B) A fixed concentration (500 nM) of cerivastatin completely overcomes MAG inhibition of ES-MN growth, but its effects are progressively canceled out by increasing concentrations of mevalonate (MVL). There is no effect of MVL on axonal growth in the absence of statins (mean ± SEM; n = 6).

(C and D) Farnesyl pyrophosphate (Fpp) (C) and geranylgeranyl pyrophosphate (GGpp) (D) can also reverse the growth-promoting effect of statins without affecting intrinsic growth rates on either Ctrl-CHO or MAG-CHO monolayers (mean ± SEM; n = 6).

(E) Mixed inhibitors of geranylgeranyl transferase (GGTI) and farnesyl transferase (FTI) enhance neurite outgrowth on MAG-CHO.

(F) More selective inhibitors (GGTI-2417 and FTI-2153) promote neurite outgrowth synergistically, since the value for increased length above baseline is more than additive (mean ± SEM; n = 6, $p < 0.001$). Note that a combination of both inhibitors drives neurite outgrowth to levels comparable to those of vehicle-treated neurons on non-inhibitory control CHO cells (unfilled bar).

pathway provide a brake on axonal growth even on the most supportive substrata.

Statins Promote Neurite Outgrowth by Inhibiting 3-Hydroxy-3-Methylglutaryl-Coenzyme A Reductase

The cognate target of all statins is the enzyme 3-hydroxy-3-methylglutaryl-coenzyme A (HMG-CoA) reductase (HMGCR), which catalyzes a rate-limiting upstream step in cholesterol biosynthesis (Figure 3A). If statins stimulate axonal growth by inhibiting HMGCR, adding back the enzyme product mevalonate (which is cell permeable) in the presence of statin should restore inhibition. Mevalonate alone had no effect on neurite growth on either control or MAG-CHO monolayers, while addition of increasing concentrations of mevalonate in the presence of a fixed 500 nM concentration of statin, itself capable of completely overcoming myelin inhibition, fully reconstituted inhibition by MAG (Figure 3B). Therefore, HMGCR inhibition accounts for all neurite-promoting actions of cerivastatin, and endogenous levels of mevalonate are not limiting for full inhibition by MAG. Nevertheless, inhibiting this pathway necessarily leads to reductions in the levels of cholesterol, which could be damaging in the CNS, where it plays multiple roles in synapse function. We therefore sought a means to mimic the biological effects of statins on axon growth without affecting cholesterol.

Inhibition of Protein Prenylation Accounts for the Statin-Induced Increase in Axonal Growth

Downstream of HMGCR, multiple branches of the mevalonate pathway lead to the synthesis of isoprenoids involved in the synthesis of cholesterol as well as lipid intermediates required for post-translational protein prenylation (Figure 3A; van der Most et al., 2009; Corsini et al., 1999). We examined the role of each in the inhibition of neurite outgrowth. The last intermediate common to all the branches is farnesyl pyrophosphate (Fpp). Using add-back experiments (Wasko et al., 2011), we confirmed that Fpp prevents growth enhancement by cerivastatin (Figure 3C). In contrast, neither coenzyme Q4 or Q10 (from the left-hand branch in Figure 3A) nor high-density lipoprotein (HDL)- or low-density lipoprotein (LDL), which affect cholesterol synthesis, reconstituted the growth inhibition (Figures S3B–S3E), demonstrating that it is not necessary to block cholesterol or coenzyme Q synthesis to enhance neurite outgrowth.

However, application of GGpp to ES-MN cultures treated with cerivastatin completely restored inhibition by MAG (Figures 3C and 3D). The strong, selective effects of Fpp and GGpp pointed to inhibition of protein prenylation as the principal mode of statin action in our system. To confirm the involvement of prenylation enzymes, we first tested small-molecule inhibitors GGTI-298

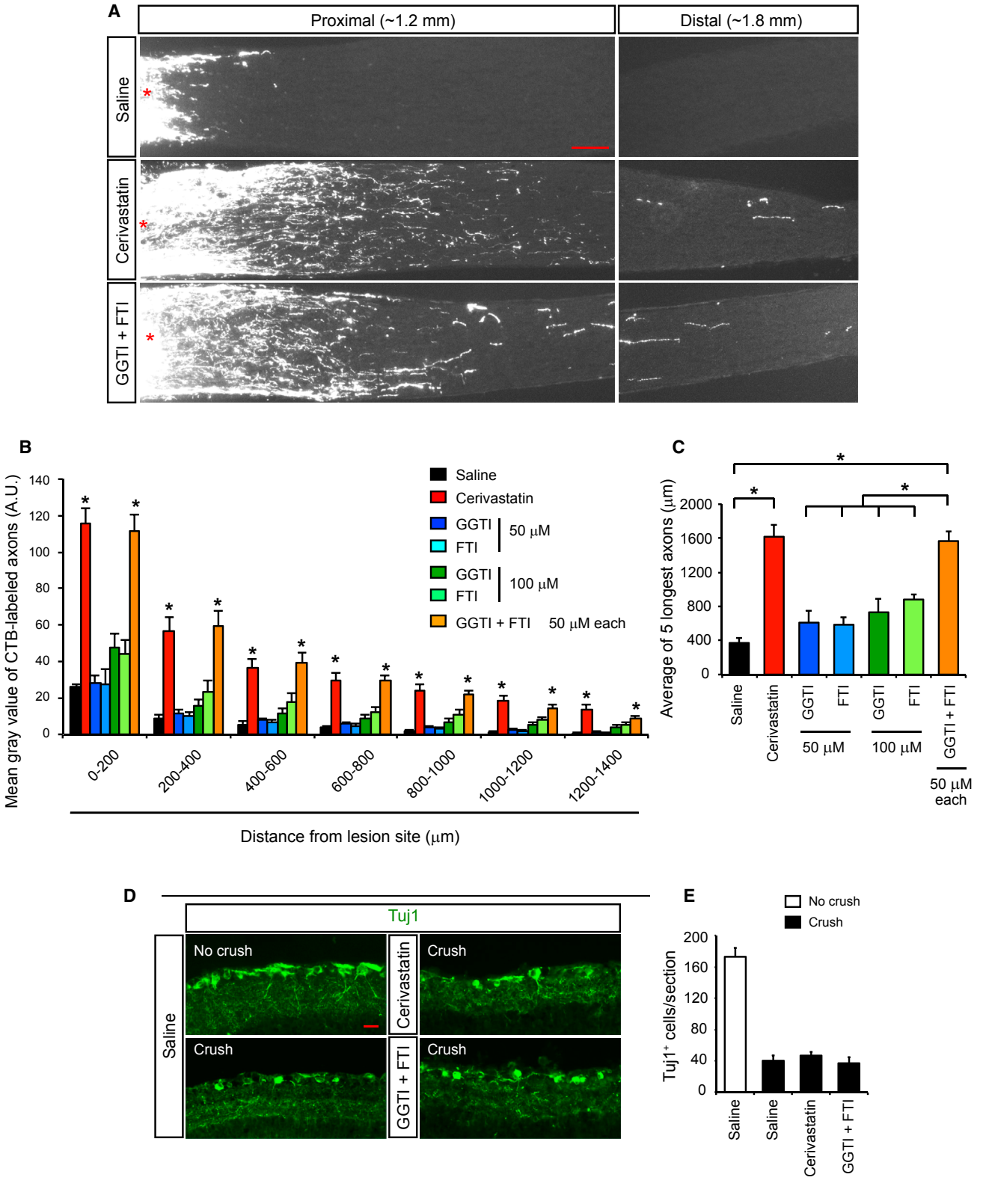

(legend on next page)

and FTI-277, each of which is incompletely selective (see Figure S3A for in vitro half-maximal inhibitory concentration (IC_{50}) values for both PGGT-1 and PFT). Both promoted neurite growth in a dose-dependent manner (GGTI-298: EC_{50} = 2.6 ± 0.21 μM, n = 7; FTI-277: 5.6 ± 0.21 μM, n = 6; Figure 3E). To determine whether one or both of the two prenylation pathways was involved, inhibitors with greater specificity for their respective targets, GGTI-2417 and FTI-2153, were tested (Figure S3A). Tested alone, GGTI-2417 had no significant effect ($p = 0.266$) whereas FTI-2153 led to a 1.7-fold increase in neurite outgrowth ($p < 0.001$; Figure 3F). Strikingly, though, their actions were strongly synergistic ($p < 0.001$ for a synergistic as opposed to additive effect; Bliss model). The combined inhibition of PGGT-1 and PFT was sufficient to induce a 3-fold increase in axon outgrowth on MAG over the 20-hr culture period (Figure 3F). The resulting growth on MAG was similar to that on control CHO cells. Therefore, inhibition of dual protein prenylation pathways can stimulate axonal growth without inhibiting cholesterol synthesis (Figure 6F).

Statins and Prenylation Inhibitors Promote CNS Axon Regeneration In Vivo

To explore the role of this mechanism in mature CNS neurons in vivo, we used the optic nerve crush model, in which compounds applied into the eye gain direct access to injured retinal ganglion cells (RGCs) (Figure 4). The optic nerve of 6- to 8-week-old mice was injured by pinching with forceps, and immediately afterward, a total volume of 2 μl saline, 25 μM cerivastatin, 50 or 100 μM GGTI-2417 (GGTI), 50 or 100 μM FTI-2153 (FTI), or a combination of 50 μM GGTI and 50 μM FTI was intravitreally injected into the peripheral zone of the eye. The final total (free + bound) concentrations of these compounds in the vitreous was estimated to be in the micromolar range. At 14 days post-injury, live regenerating axons were labeled by anterograde tracing using labeled cholera toxin β-subunit and fixed 3 days later (Figure 4A). We confirmed that the same axons expressed GAP-43, a marker of regenerating axons (Figure S4; Koprivica et al., 2005). Mice treated with saline showed few regenerating axons distal to the lesion site (Figure 4A). However, following treatment with cerivastatin, robust regrowth of RGC axons was observed (average of five longest axons: saline = 371 ± 64 μm versus cerivastatin = 1,618 ± 137 μm, $p < 0.01$; Figures 4A and 4C). To provide a more complete measure, we quantified cholera toxin B subunit (CTB) labeling on serial sections of optic nerves at different distances from the lesion (Figure 4B). There was a highly significant effect ($p < 0.01$) of cerivastatin as compared to saline control at all positions in the nerve. Following nerve crush in 24-week-old mice, statin treatment also conferred benefit (not shown).

We next asked whether, as in vitro, prenylation inhibitors could mimic the beneficial effect of statins. Effects of the combination of 50 μM GGTI-2417 and 50 μM FTI-2153 were indistinguishable from that of cerivastatin, at all distances from the lesion (Figures 4A–4C). Strikingly, neither of the inhibitors used singly had a robust effect on optic nerve regeneration, making the synergistic effect of the combination highly significant ($p < 0.01$; Figure 4C). One possible explanation of the increased axonal growth might have been protection of RGCs from injury-induced death, which we determined to be 77% after 2 weeks in saline-treated mice (Figures 4D and 4E). However, no neuroprotective effect of either cerivastatin or a combination of GGTI + FTI was observed (Figures 4D and 4E), suggesting that both agents act primarily to enhance growth of regenerating CNS axons in vivo.

Significance of the Mevalonate and Prenylation Pathway for Axonal Degeneration and Regeneration in Human Patients with ALS

All experiments thus far had used mouse models. We therefore tested inhibitors on two systems of human stem cell-derived motor neurons: the "gold-standard" ES-derived motor neurons expressing an Hb9::GFP reporter as well as human induced pluripotent stem cell-derived motor neuron (hiPS-MNs) derived from ALS patients and controls (Amoroso et al., 2013, Boulting et al., 2011, Maury et al., 2015). Human neurons grew well on control CHO cells and, like their mouse counterparts, showed clear growth inhibition on a MAG-CHO cell monolayer (Figure 5A) but little reduction in survival (values for MAG-CHO were 89%–92% of those on control CHO cells). Addition of cerivastatin led to a dose-dependent, 6-fold increase in axon length over the 20-hr culture period (Figures 5A and 5B). The fold-increase of neurite length was even stronger than on mouse motor neurons, though the EC_{50} was higher (390 ± 56 nM; n = 6). Hb9::GFP motor neurons in mixed cultures (~30% abundance) or purified by FACS responded in a comparable manner to cerivastatin (Figure 5B). Introduction of an ALS-causing point mutation into the *SOD1* gene of the same ES line only modestly reduced the ES-MN response to statins (Figure 5C). To directly confirm that statins can affect human ALS motor neurons, we generated hiPS-MNs from the 007 human induced pluripotent stem cell (hiPSC) line derived from a patient with an $SOD1^{A4V}$ point mutation, as well as an isogenic control line in which the mutation had been corrected (Figure 5D). Cerivastatin strongly promoted neurite outgrowth from both, and once again, ALS motor neurons

Figure 4. Both Cerivastatin and a Combination of Prenylation Inhibitors Strongly Promote Retinal Axon Regeneration In Vivo

(A) Enhancement of retinal axon regeneration by cerivastatin and protein prenylation inhibitors, GGTI-2417 (GGTI) and FTI-2153 (FTI) administered intravitreally at the time of lesion GGTI-2417 (GGTI). 10-μm cryosections through optic nerve 14 days later show increased numbers of CTB-labeled regenerating axons distal to the injury site in cerivastatin or (GGTI + FTI)-treated mice as compared to saline.

(B and C) Quantitative analysis of regrowing axons in saline, cerivastatin, or protein prenylation inhibitor-treated mice. Mean gray values of CTB-labeled regenerating axons in 200-μm columns progressively further from the lesion site obtained at constant illumination are shown in a.u. in (B), and the distance from the lesion site of the five longest axons was analyzed in (C). Note that cerivastatin or combinations of GGTI and FTI led to ~4-fold increases in retinal axon regrowth by either measure. All data from quantification of axon regeneration are expressed as mean ± SEM; n = 4 for saline, n = 5 for 25 μM cerivastatin, n = 4 for 50 μM GGTI, n = 4 for 50 μM FTI, n = 3 for 100 μM GGTI, n = 3 for 100 μM FTI, and n = 6 for 50 μM GGTI + 50 μM FTI. *$p < 0.01$.

(D and E) No effect on RGC survival of either cerivastatin or protein prenylation inhibitors after optic nerve injury. 10-μm cryosections through the retina show $Tuj1^+$ RGCs (D), and quantitative analysis of the number of $Tuj1^+$ RGCs in saline, cerivastatin, or prenylation inhibitors (GGTI + FTI)-treated mice with or without optic nerve injury in (E). All data in (E) are expressed as mean ± SEM; n = 3 for each condition. Scale bars represent 100 μm in (A) and 20 μm in (D).

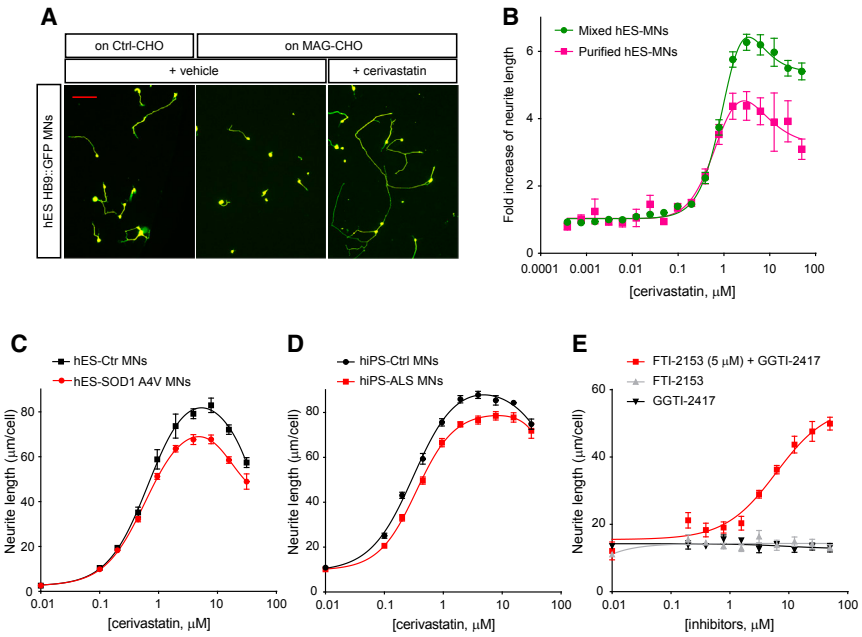

Figure 5. Human-Patient-Derived Motor Neurons Show Strong Axonal Growth Responses to Statins and Prenylation Inhibitors

(A) Images of human ES-MNs expressing Hb9::GFP grown on control-CHO and MAG-CHO with and without cerivastatin. Scale bars, 100 μm.

(B) Mixed and purified human ES-MNs similarly overcome MAG-induced neurite inhibition in the presence of cerivastatin with a 6-fold increase in neurite length in the first 20 hr of culture.

(C and D) Cerivastatin also has marked axonal growth effects on (C) human ES-MNs with or without an $SOD1^{A4V}$ mutation knocked in using zinc-finger technology and (D) hiPS-MNs from a healthy control or $SOD1^{A4V}$ ALS patient.

(E) Combinations of GGTI-2417 and FTI-2153 overcome inhibition of neurite outgrowth of hiPS-MNs by MAG-CHO, whereas GGTI or FTI alone show no effect. Values are plotted as mean ± SEM; n = 6 replicates. Data are representative of at least three independent preparations of ES/hiPS-MNs.

responded similarly to their control counterparts. Effects on survival were minor (<50% increase in the presence of statins as compared to >600% for neurite outgrowth).

Lastly, we tested the prenylation inhibitors GGTI-2417 and FTI-2153, alone and in combination, on hiPS-MNs from the 18c healthy control line (Lamas et al., 2014) grown on MAG-CHO cells (Figure 5E). Their synergistic effects were striking; neither compound tested alone significantly stimulated axon growth, but in combination, they triggered a 3-fold increase over the first 20 hr of culture.

To determine whether protein prenylation might also regulate growth in adult human motor neurons in vivo, we turned to a published microarray analysis of lumbar motor neurons that were laser captured from ALS patients who had died of the bulbar form of the disease, meaning that many motor neurons still survived at the less-affected lumbar levels (Rabin et al., 2010). We interrogated the normalized raw expression data for all enzymes in the mevalonate and prenylation pathways, asking whether there might be differences between ALS and controls, or between early- and late-onset cases in the cohort of 12 ALS patients studied. Levels of most enzymes in the pathway showed no significant correlation with age, or difference between early- versus late-onset ALS (cutoff defined as 60 years; Figure 6A). The same was true of many other pathways tested (not shown), suggesting that there was no significant age-dependent methodology bias within the dataset. HMGCR, PFT, and PGGT-2 did not show any variation with age or disease state (Figures 6B–6D). However, one prenylation enzyme showed a striking correlation. In control motor neurons, *PGGT1B*, the gene that encodes PGGT-1, β subunit showed no significant variation with age. In contrast, in motor neurons from ALS patients, its levels were higher (~6-fold) than controls in early-onset cases and diminished linearly with age (R^2 = 0.62) to reach control levels in older patients. Despite the small numbers of patients analyzed, these differences were highly significant (p = 0.01 for early versus late onset; p = 0.002 for correlation with age). Importantly, this observation was motor-neuron specific, since *PGGT1B* expression in the dorsal spinal cord of the same ALS patients showed no correlation with age or disease state (data not shown; Rabin et al., 2010). The only other two mevalonate pathway genes to show a degree of correlation with age were ACAT1 and MVD (Figure 6A). However, the difference in expression levels between early- and late-onset ALS was low (<1.5-fold for both genes), suggesting that the functional impact was not significant.

DISCUSSION

Our understanding of the cell-intrinsic mechanisms that regulate neurite growth remains incomplete. In particular, there is a critical need for a means by which to enhance axonal regeneration in human patients. By conducting an extensive screen for small molecules able to overcome myelin inhibition, we found that statins are the most potent neurite growth-promoting agents yet reported, both for rodent and human neurons. Moreover, comparable effects on axonal regeneration can be generated, without blocking cholesterol synthesis, by inhibiting both branches of the protein prenylation pathway, either in vitro or in vivo. In all neurons examined, we found that endogenous levels of prenylation are maintained at a level that constitutes a brake on axonal growth, and expression data suggest this may contribute to lack of compensatory sprouting in early-onset ALS patients. Targeting the mevalonate-prenylation pathway may therefore allow both preventive and reparative approaches in human patients with CNS trauma or neurodegenerative disease.

Other screens reported to date have used different cellular models and ~20-fold-smaller screening libraries (Al-Ali et al.,

A

Gene symbol	Gene Name	p value correlation	p value early vs late
ACAT1	Acetoacetyl-CoA transferase ACAT1	0.008	0.05
ACAT2	Acetoacetyl-CoA transferase ACAT2	0.653	0.56
HMGCS1	HMG-CoA synthase1	0.884	0.91
HMGCS2	HMG-CoA synthase2	0.372	0.23
HMGCR	HMG-CoA reductase	0.915	0.83
MVK	Mevalonate kinase	0.220	0.42
PMVK	Phosphomevalonate kinase	0.344	0.29
MVD	Mevalonate-5-pyrophophate decarboxylase	0.030	0.05
IDI1	Isopentenyl-diphosphate isomerase 1	0.751	0.80
FDPS	Farnesyl diphosphate synthase	0.906	0.86
FNTA	Farnesyl transferase alpha subunit	0.213	0.12
FNTB	Farnesyl transferase beta subunit	0.985	0.96
GGPS1	Geranylgeranyl diphosphate synthase	0.139	0.19
PGGT1B	Geranylgeranyl transferase beta subunit	0.002	0.01
RABGGTA	Rab geranylgeranyl transferase, alpha subunit	0.534	0.36
RABGGTB	Rab geranylgeranyltransferase, beta subunit	0.093	0.31

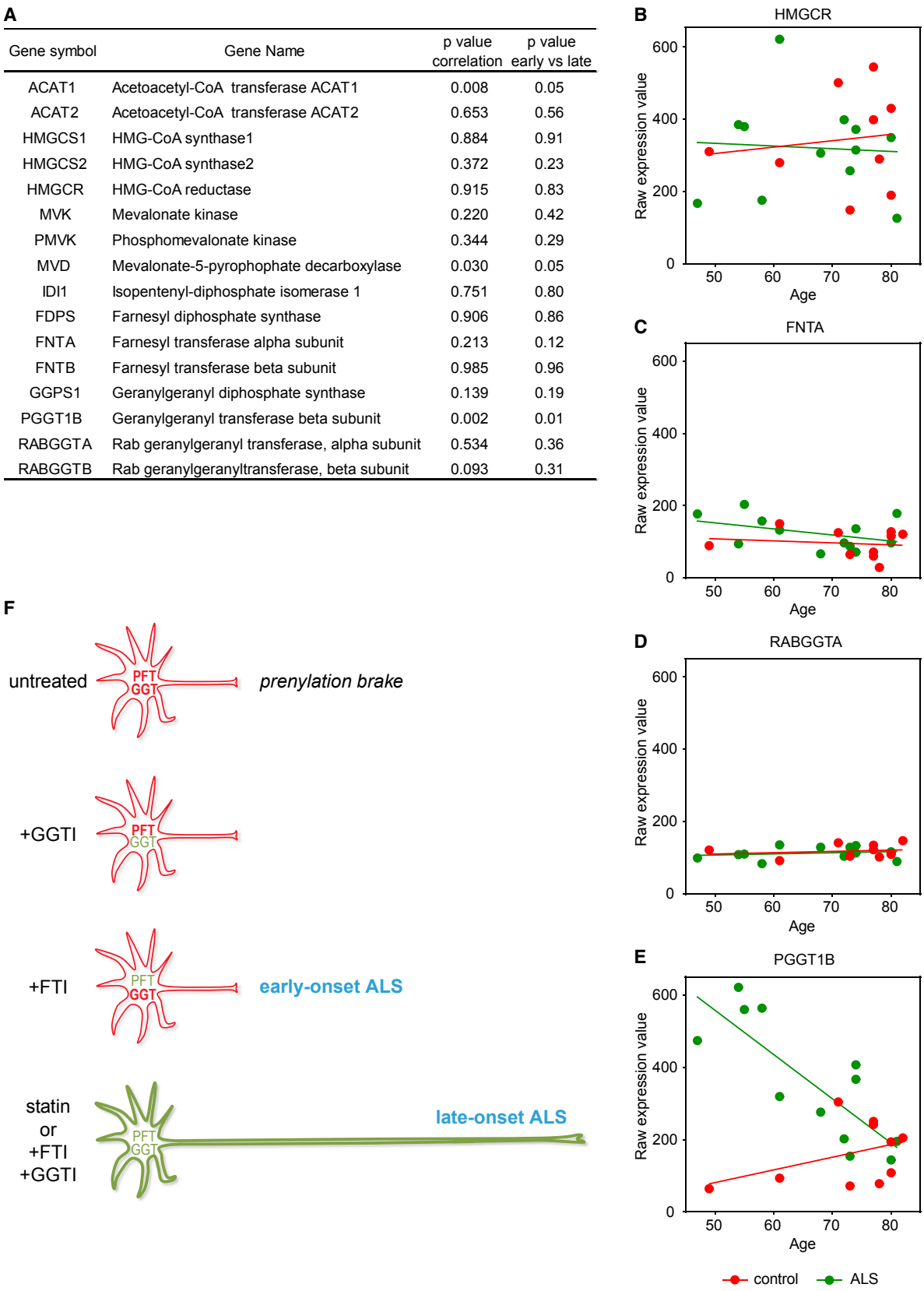

(legend on next page)

2015; Ma et al., 2010; Usher et al., 2010; Koprivica et al., 2005). Likely reflecting these differences, in our system, we could not detect activity of either daidzein, which has already been reported to work only when neurons are primed by pre-exposure to drug (Ma et al., 2010), or erlotinib (Koprivica et al., 2005; Figure S1D). In our hands, despite the specific nature of our screening model, statins were effective on all neurons (both stem cell derived and primary) and all substrata (both inhibitory and permissive) tested. They seem therefore to trigger a general boost in axon growth potential.

The tissue that expresses the highest levels of HMGCR is the brain (Burkhardt et al., 2008). Multiple and often contradictory effects of statins and prenylation inhibitors on cultured neurons have been reported. These include changes in directional growth of axons without any increase in axonal length (Holmberg et al., 2006), protection of axons against excitotoxicity (Posada-Duque et al., 2013), decreased neurite length (Schulz et al., 2004, Kim et al., 2009), or no effect (Fan et al., 2002). The data most comparable to ours are those of Pooler et al. (2006), who report a 40% increase in neurite length of hippocampal neurons following exposure to high concentrations ($\geq$100 μM) of pravastatin or 50 μM GGTI-286, but not FTI-277. But these concentrations, which are at least an order of magnitude above the EC_{50}, were found to be toxic in our study and other studies (Figures 2C, 2D, and 3E; Butterfield et al., 2011). It is unclear whether these disparities are due to specificities of neurons and substrata or the methodology of quantification and cell culture, and in vivo validation is therefore critical. Our finding that a single intravitreal injection of statin or prenylation inhibitors was sufficient to support RGC axonal growth over 2 weeks at levels comparable with many genetic manipulations was highly encouraging. It is reasonable to suppose that the effect will be still greater when the drug can be delivered continuously and in the presence of an agent that prevents the >75% loss of RGCs caused by axotomy and not rescued by cerivastatin.

Inhibition of protein prenylation is considered to play a key role in many biological effects of statins not directly linked to cholesterol (Samuel and Hynds, 2010). Hundreds of intracellular signaling proteins (e.g., small GTP/GDP-binding proteins) may potentially be prenylated, but only a minority of modifications have been specifically identified (Samuel and Hynds, 2010; Charron et al., 2013). Some, like K-Ras, Ras, and H-Ras, are exclusively farnesylated, while others, such as Rac, Rho, and Rap, are geranylgeranylated; lastly, one (RhoB) is modified by both enzymes (Zhang and Casey, 1996). We found both in vitro and in vivo that inhibiting both farnesylation and geranylgeranylation provided the strongest benefit for axonal growth. This may suggest a central role for a doubly modified protein, or it may mean that multiple prenylation substrates are involved. Distinguishing between such possibilities is complicated. First, compensatory prenylation has also been described; when PFT is inhibited by FTIs, K-Ras and N-Ras, but not H-Ras, become geranylgeranylated. Second, knockdown or inhibition of Rac1 was shown to mimic the neuroprotective actions of statins on cortical neurons (Posada-Duque et al., 2013), yet a non-prenylatable mutant of Rac1 was recently shown to retain its function in a neurite outgrowth assay (Reddy et al., 2015).

Given the widespread usage of statins, many authors have addressed the question of whether they are protective and/or beneficial in CNS indications. Citing only the most recent meta-analyses for multiple sclerosis, cognition in Alzheimer's disease, and Parkinson's disease, the response is unclear (Pihl-Jensen et al., 2015; Chatterjee et al., 2015; Huang et al., 2015), although there are signs that statin use in patients with intracerebral hemorrhage may be associated with improved mortality and functional outcomes (Jung et al., 2015). One reason for inconsistency or lack of effect is the very limited information we have on brain exposure and pharmacodynamics for statins in general. It is generally considered that lipophilic statins like simvastatin lactone cross the blood-brain barrier, whereas atorvastatin, which is relatively less lipophilic, does not (Serajuddin et al., 1991). However, we performed a pharmacokinetic study (not shown) for cerivastatin and simvastatin and found both to have extremely short half-lives in rodents, whether administered centrally or peripherally.

Patients expected to have high endogenous levels of prenylation in their motor neurons, through higher expression of *PGGT1B*, showed earlier ALS onset, perhaps due to their reduced ability to reinnervate denervated muscle fibers (see model in Figure 6F). We did not find a difference in basal outgrowth between the ALS and control hiPS-MNs we analyzed in vitro. However, this was not unexpected, since hiPS-MNs are embryonic in phenotype and have not been exposed to the multiple epigenetic influences that may lead to changes in gene

Figure 6. Levels of *PGGT1B* Are Selectively Elevated in Motor Neurons of Patients with Early-Onset ALS as Compared to Late-Onset Patients or Healthy Controls

(A) Based on the raw data of Rabin et al. (2010), for each enzyme in the different branches of the mevalonate pathway, we calculated the significance of the overall difference between ALS and control patients (p value correlation) and the difference between the values in early-onset (<60 years) and late-onset (>60 years) ALS patients (p value early versus late). Only *PGGT1B*, which encodes the β subunit of PGGT-1, showed a significant correlation with age of onset as well as a significant fold-difference in expression levels between early- and late-onset cases.

(B–E) Scatterplots of expression levels of individual genes analyzed in this study in ALS patients (green) and controls (red). Whereas ALS and control values were indistinguishable for the first three genes (with some scatter for HMGCR), early-onset patients expressed high levels of PGGT1B that decreased progressively (R^2 = 0.62) with increasing age. No similar change was seen in healthy controls over the same age range or in dorsal spinal neurons from the same ALS patients (not shown).

(F) Model showing how prenylation enzymes provide a double brake on axonal growth. Levels of PFT and PGGT-1 are high (bold red font) in untreated neurons in vitro and in vivo. Reducing activity or expression level (normal green font) of a single enzyme is not sufficient to completely remove the brake, whereas inhibiting both, using either statins or combinations of prenylation inhibitors, leads to a >3-fold increase in axonal length. Laser-capture microarray profiling suggests that motor neurons from early-onset ALS cases have high levels of PGGT-1 but low levels of PFT; this may not be sufficient to allow regenerative axonal sprouting. The low levels of both enzymes in motor neurons from late-onset ALS cases are consistent with their having delayed the onset of physical manifestations through their ability to sprout and reinnervate denervated muscle fibers.

expression in adult human neurons. Based on our data, one hypothesis would be that patients taking statins would show a greater propensity for compensatory axonal sprouting, meaning that with a given risk from other causes, they would either develop ALS later or not at all. Although earlier meta-analyses were not conclusive (Zheng et al., 2013), a recent large study (722 ALS patients and 2,268 controls) showed evidence for a protective effect of statins against the onset of ALS (Seelen et al., 2014). In accordance with our hypothesis, the major contributor to the improved odds ratio was simvastatin, which is considered the most brain penetrant of the statins.

Our data show that neurons in multiple contexts maintain endogenous levels of prenylation that restrict their maximum growth capacity. In the adult CNS, exuberant sprouting might lead to circuit dysfunction and behavioral abnormalities. However, it is less clear why embryonic neurons growing on permissive substrata would need a brake on their growth. One intriguing possibility is raised by studies of extracellular signaling molecules such as semaphorins, which control not only the direction but also the timing of axon growth to specific territories during embryogenesis (Huber et al., 2005). Therefore, activity of the mevalonate-prenylation pathway may potentially govern the establishment of neural circuits in a cell-intrinsic manner.

Overall, our data support the idea that the mevalonate-prenylation pathway represents a target for therapeutic approaches to currently incurable diseases and trauma of the CNS. Although the small molecules currently available to target the pathway have limitations in terms of bioavailability and rare on-target toxicity (Cziraky et al., 2013), the exceptional potency of the effects they engender in model systems suggests that therapeutic strategies to inhibit prenylation should be pursued for currently incurable diseases such as ALS.

EXPERIMENTAL PROCEDURES

mES-MN and hiPS-MN Differentiation

Mouse ESCs carrying the *Hb9::GFP* transgene were differentiated into motor neurons as described previously (Wichterle et al., 2002). Human ES-MNs and hiPS-MNs from healthy control and ALS patients were differentiated as described in Lamas et al. (2014) (Amoroso et al., 2013; Boulting et al., 2011; Maury et al., 2015). Briefly, human ESC colonies were cultured in ESC medium with 20 ng/ml basic fibroblast growth factor (bFGF) for 4 days before they were switched to neural induction medium (DMEM/F12 medium with 1 μM retinoic acid and 10 ng/ml brain-derived neurotrophic factor [BDNF]). Medium was replaced after 4 days and replenished with 1 μM retinoic acid and 200 ng/ml sonic hedgehog protein (SHH) for 13 days. Embryoid bodies were cultured for another 10 days in neural differentiation medium (Neurobasal medium supplemented with 1 μM retinoic acid, 200 ng/ml SHH, 2% B-27 supplement [Invitrogen], 10 ng/ml BDNF, 10 ng/ml ciliary neurotrophic factor (CNTF), 10 ng/ml glial cell line-derived neurotrophic factor (GDNF), and 10 ng/ml IGF-1) before they were dissociated.

Purified Hb9::GFP human ES-MNs were sorted based on GFP expression using a BD FACS Aria II sorter (Becton Dickinson) under low-pressure conditions for 30 min. 1,000–2,000 purified GFP-positive cells were plated onto MAG-CHO cell monolayer in each of the 96 wells.

Neurite Outgrowth Assay on MAG or CSPG

Confluent monolayers of control and MAG-expressing CHO cells were established over a 24-hr period in 96-well microplates with transparent bases (Greiner Bio One). Embryoid bodies were dissociated, and 2,500 mature ES-MNs were plated onto monolayers in each well in Neurobasal medium (catalog no. 21103-049 without phenol red, without riboflavin) containing B27 2% glutamine 0.5 mM, glutamate 0.025 mM, β-mercaptoethanol 0.1%, and CNTF 10 ng/ml. For CSPG inhibition, microplates were coated with poly-D-ornithine (100 μg/ml) and laminin (3 μg/ml). ES-MNs were seeded, and CSPG was added to the neuronal cultures at 10 μg/ml. After 18–20 hr, whole-well images of GFP-positive ES-MNs were captured using a Flash Cytometer (Trophos) and analyzed for average neurite length per cell using MetaMorph (Molecular Devices) image analysis software. Detailed procedures for imaging and analyzing other neuronal cell types are listed in the Supplemental Experimental Procedures.

High-Throughput Screen

Compounds were added to the ES-MN culture at final concentration of 10 μM with 0.5% DMSO.

Neurite outgrowth data were converted to fold change by normalizing them to mean neurite length of the six negative controls (mock treatment with blank vehicle) in each plate. Compounds that gave values >1.3-fold those of negative controls were picked as putative hits, and images of those data points were visually screened to remove false positives caused by auto-fluorescence. The primary hits were then tested in a duplicated five-point 2-fold dilution series. Compounds that showed >30% enhancing effect were purchased from original vendors and tested in a nine-point 2-fold dilution series in six replicates. Compounds that showed >80% enhancing effect consistently were identified as the leads.

Chemical Libraries

Using this assay, we first performed a pilot screen of a small library of 2,000 bioactive compounds including US Food and Drug Administration (FDA)-approved and natural compounds (MicroSource) (Figure 1E). Subsequently, we screened two other libraries, TIC and BBB, developed by the Stockwell lab (Columbia University). The TIC library was assembled from natural product libraries purchased from commercial sources and was designed by selecting several chemical features according to the following rules: (1) limit the number of steroids, which are heavily studied and can have pleiotropic effects; (2) maximize the number of chiral centers and therefore the structural complexity; and (3) minimize unsaturated rings that are less abundant in natural products. Compounds in the BBB library were specifically selected to be drug-like and likely to cross the blood-brain barrier as defined by an in silico filtering protocol (Brent Stockwell, unpublished data). Compounds with predicted logBB values (logarithm of the brain-to-blood partitioning ratio) greater than zero (on a log scale from −3 to +6) were selected first. Of these compounds, those with molecular weights <250 or containing more than two aromatic rings were discarded to eliminate very simple compounds and highly fluorescent or planar compounds that might intercalate into DNA.

Optic Nerve Crush and Intravitreal Injection

All animal procedures followed the regulatory guidelines of the Columbia University Institutional Animal Care and Use Committee. The optic nerve crush and the intravitreal injection in 6- to 8-week-old mice were performed as described previously (Park et al., 2008). After the nerve crush, 2 μl of saline or cerivastatin, GGTI-2417, FTI −2153 or combinations of GGTI-2417 and FTI-2153 at different concentrations was intravitreally injected into the peripheral retina. Each compound (2 μl) is diluted 1:10 in the vitreous based on the fact that the vitreous volume is 20 μl (Saszik et al., 2002). 14 days after injury, 2 μl cholera toxin β subunit coupled to Alexa Fluor 555 (CTB-555) (1 μg/μl, Life Technologies) was intravitreally injected into the retina. 3 days after CTB injection, the eye with optic nerve was dissected out, post-fixed in 4% PFA overnight, and cryoprotected in 30% sucrose in PBS. Eye and optic nerves were separately frozen on dry ice, and 10-μm cryosections were prepared for axon regeneration and RGC survival analysis.

Automated Quantification of Axon Regeneration and RGC Survival

To quantify CTB-labeled regenerating axons, three cryosections of ~2 mm optic nerve per animal were washed with PBS and mounted with an aqueous mounting medium. CTB-labeled regenerating axons were imaged in grayscale using a constant exposure time. In each section, ImageJ provided a mean gray value of CTB-labeled axons in each 200-μm optic nerve column from the lesion

site after removing the value on background (non-tissue area) in the same image. The average of mean gray value of regenerating axons in each 200-μm optic nerve column was obtained from three sections per animal. Each condition was tested with three to six animals (n = 3–6). To obtain length of the five longest axons, the distance of the five longest axon tips from the injury site was measured with ImageJ in each section. The average of the five longest axons was obtained from three sections per animal. Each condition was tested with three to six animals (n = 3–6). To examine RGC survival, the 60^{th}–80^{th} sections of −150 sagittal cryosections of the whole retina per animal were immunostained with anti-β-III tubulin antibody. Five sections among them were selected randomly for the analysis. After counting the number of $Tuj1^+$ cells in all five sections per animal, the average number of β-III $tubulin^+$ cells in the retina per animal was obtained, and it was pursued repeatedly with three animals in the same condition (n = 3).

Analysis of Gene Expression Data from Postmortem ALS

The expression data were generated on the Affymetrix HuEx_1_0_st_v2 chip and normalized using the robust multi-array average (RMA) method. To test how the expression levels of a gene of interest vary with age (at death/sample collection) in ALS patients or healthy controls, a linear model was fitted between the log-intensity values and the age at sample collection. Disease duration did not vary significantly among the ALS patients, and the age at onset and age at death were highly correlated (data not shown). The R^2 (unadjusted) and p values of the coefficient for age in this model are reported in Figure 6A (column 3). To test whether the genes of interest are expressed differentially between late-onset and early-onset ALS patients, a linear model was fit between the log-intensity values and the ALS categorization (early, late, or control). The p values of the coefficients in this fit are reported in Figure 6A (column 4). Since the above analyses were done on genes comprising the mevalonate pathway (<20 genes) only, we report only the unadjusted p values. All analyses were done in the statistical language R.

SUPPLEMENTAL INFORMATION

Supplemental Information includes Supplemental Experimental Procedures and four figures and can be found with this article online at http://dx.doi.org/10.1016/j.celrep.2016.06.013.

AUTHOR CONTRIBUTIONS

H.L. conducted experiments, analyzed data, and wrote the manuscript. T.K. performed and analyzed optical nerve crush experiments and wrote the manuscript. D.O. and R.H. analyzed gene expression data. E.N. performed experiments with hippocampal neurons and analyzed optic nerve crush experiments. J.H. performed optic nerve crush experiments. W.S.Y. provided support for the compound libraries. E.R.L., N.J.L., M.W.A., G.F.C., and H.W. provided ES or hiPS cell-derived motor neurons. S.S. provided specific prenylation inhibitors and contributed to the writing of the manuscript. M.T.F. coordinated research efforts and provided the CHO cells. B.S. coordinated research efforts, provided the compound libraries, and contributed to the writing of the manuscript. C.E.H. coordinated research efforts, supervised research work and data analysis, and wrote the manuscript.

ACKNOWLEDGMENTS

We thank Samaher Fageiry and Cyndel Vollmer for help with the culture model, Kevin Eggan and collaborators for kindly providing Hb9::GFP human ESC reporter lines, and Chuck Karan and members of the High-Throughput Screening and Chemistry Shared Facility for support and technical guidance. We thank the He lab (Harvard) for training in optic nerve crush. We are grateful to members of the Project A.L.S., Henderson, Wichterle, and Stockwell laboratories at Columbia University for much help and continuous critical discussion. We thank our Biogen colleagues Alex McCampbell, Sha Mi, and Richard Ransohoff for critical reading of the manuscript. This work received invaluable support from the New York State Spinal Cord Injury Research Board (NYSSCIRB C020923), P2ALS, Target ALS, the Tow Foundation, the SMA Foundation, Project A.L.S., NYSTEM (C026715), The Helmsley Charitable Trust, NINDS R01-NS056422 and NS072428, and the Columbia MD-PhD program. Brent R. Stockwell is an Early Career Scientist of the Howard Hughes Medical Institute, and this research was additionally funded by the NIH (5R01CA097061 and R01CA161061, to B.S.) and New York State Stem Cell Science (C026715).

This article is dedicated to the memory of our dear friend and colleague Marie T. Filbin, a trailblazer in the field of axonal regeneration.

Received: October 20, 2015
Revised: January 31, 2016
Accepted: May 28, 2016
Published: June 30, 2016

REFERENCES

Al-Ali, H., Lee, D.H., Danzi, M.C., Nassif, H., Gautam, P., Wennerberg, K., Zuercher, B., Drewry, D.H., Lee, J.K., Lemmon, V.P., and Bixby, J.L. (2015). Rational polypharmacology: systematically identifying and engaging multiple drug targets to promote axon growth. ACS Chem. Biol. *10*, 1939–1951.

Alizadeh, A., Dyck, S.M., and Karimi-Abdolrezaee, S. (2015). Myelin damage and repair in pathologic CNS: challenges and prospects. Front. Mol. Neurosci. *8*, 35.

Amoroso, M.W., Croft, G.F., Williams, D.J., O'Keeffe, S., Carrasco, M.A., Davis, A.R., Roybon, L., Oakley, D.H., Maniatis, T., Henderson, C.E., and Wichterle, H. (2013). Accelerated high-yield generation of limb-innervating motor neurons from human stem cells. J. Neurosci. *33*, 574–586.

Baas, P.W., and Matamoros, A.J. (2015). Inhibition of kinesin-5 improves regeneration of injured axons by a novel microtubule-based mechanism. Neural Regen. Res. *10*, 845–849.

Bordet, T., Buisson, B., Michaud, M., Drouot, C., Galéa, P., Delaage, P., Akentieva, N.P., Evers, A.S., Covey, D.F., Ostuni, M.A., et al. (2007). Identification and characterization of cholest-4-en-3-one, oxime (TRO19622), a novel drug candidate for amyotrophic lateral sclerosis. J. Pharmacol. Exp. Ther. *322*, 709–720.

Boulting, G.L., Kiskinis, E., Croft, G.F., Amoroso, M.W., Oakley, D.H., Wainger, B.J., Williams, D.J., Kahler, D.J., Yamaki, M., Davidow, L., et al. (2011). A functionally characterized test set of human induced pluripotent stem cells. Nat. Biotechnol. *29*, 279–286.

Buckett, L., Ballard, P., Davidson, R., Dunkley, C., Martin, L., Stafford, J., and Mctaggart, F. (2000). Selectivity of ZD4522 for inhibition of cholesterol synthesis in hepatic versus non-hepatic cells. Atherosclerosis *151*, 41.

Burkhardt, R., Kenny, E.E., Lowe, J.K., Birkeland, A., Josowitz, R., Noel, M., Salit, J., Maller, J.B., Pe'er, I., Daly, M.J., et al. (2008). Common SNPs in HMGCR in micronesians and whites associated with LDL-cholesterol levels affect alternative splicing of exon13. Arterioscler. Thromb. Vasc. Biol. *28*, 2078–2084.

Butterfield, D.A., Barone, E., and Mancuso, C. (2011). Cholesterol-independent neuroprotective and neurotoxic activities of statins: perspectives for statin use in Alzheimer disease and other age-related neurodegenerative disorders. Pharmacol. Res. *64*, 180–186.

Cai, D., Shen, Y., De Bellard, M., Tang, S., and Filbin, M.T. (1999). Prior exposure to neurotrophins blocks inhibition of axonal regeneration by MAG and myelin via a cAMP-dependent mechanism. Neuron *22*, 89–101.

Cai, D., Deng, K., Mellado, W., Lee, J., Ratan, R.R., and Filbin, M.T. (2002). Arginase I and polyamines act downstream from cyclic AMP in overcoming inhibition of axonal growth MAG and myelin in vitro. Neuron *35*, 711–719.

Case, L.C., and Tessier-Lavigne, M. (2005). Regeneration of the adult central nervous system. Curr. Biol. *15*, R749–R753.

Charron, G., Li, M.M., MacDonald, M.R., and Hang, H.C. (2013). Prenylome profiling reveals S-farnesylation is crucial for membrane targeting and antiviral activity of ZAP long-isoform. Proc. Natl. Acad. Sci. USA *110*, 11085–11090.

Chatterjee, S., Krishnamoorthy, P., Ranjan, P., Roy, A., Chakraborty, A., Sabharwal, M.S., Ro, R., Agarwal, V., Sardar, P., Danik, J., et al. (2015). Statins and cognitive function: an updated review. Curr. Cardiol. Rep. *17*, 4.

Corsini, A., Bellosta, S., Baetta, R., Fumagalli, R., Paoletti, R., and Bernini, F. (1999). New insights into the pharmacodynamic and pharmacokinetic properties of statins. Pharmacol. Ther. *84*, 413–428.

Cziraky, M.J., Willey, V.J., McKenney, J.M., Kamat, S.A., Fisher, M.D., Guyton, J.R., Jacobson, T.A., and Davidson, M.H. (2013). Risk of hospitalized rhabdomyolysis associated with lipid-lowering drugs in a real-world clinical setting. J. Clin. Lipidol. *7*, 102–108.

Dickendesher, T.L., Baldwin, K.T., Mironova, Y.A., Koriyama, Y., Raiker, S.J., Askew, K.L., Wood, A., Geoffroy, C.G., Zheng, B., Liepmann, C.D., et al. (2012). NgR1 and NgR3 are receptors for chondroitin sulfate proteoglycans. Nat. Neurosci. *15*, 703–712.

Fan, Q.W., Yu, W., Gong, J.S., Zou, K., Sawamura, N., Senda, T., Yanagisawa, K., and Michikawa, M. (2002). Cholesterol-dependent modulation of dendrite outgrowth and microtubule stability in cultured neurons. J. Neurochem. *80*, 178–190.

Filbin, M.T. (2003). Myelin-associated inhibitors of axonal regeneration in the adult mammalian CNS. Nat. Rev. Neurosci. *4*, 703–713.

Fournier, A.E., Takizawa, B.T., and Strittmatter, S.M. (2003). Rho kinase inhibition enhances axonal regeneration in the injured CNS. J. Neurosci. *23*, 1416–1423.

Haque, S.A., Hasaka, T.P., Brooks, A.D., Lobanov, P.V., and Baas, P.W. (2004). Monastrol, a prototype anti-cancer drug that inhibits a mitotic kinesin, induces rapid bursts of axonal outgrowth from cultured postmitotic neurons. Cell Motil. Cytoskeleton *58*, 10–16.

Holmberg, E., Nordstrom, T., Gross, M., Kluge, B., Zhang, S.X., and Doolen, S. (2006). Simvastatin promotes neurite outgrowth in the presence of inhibitory molecules found in central nervous system injury. J. Neurotrauma *23*, 1366–1378.

Huang, X., Alonso, A., Guo, X., Umbach, D.M., Lichtenstein, M.L., Ballantyne, C.M., Mailman, R.B., Mosley, T.H., and Chen, H. (2015). Statins, plasma cholesterol, and risk of Parkinson's disease: a prospective study. Mov. Disord. *30*, 552–559.

Huber, A.B., Kania, A., Tran, T.S., Gu, C., De Marco Garcia, N., Lieberam, I., Johnson, D., Jessell, T.M., Ginty, D.D., and Kolodkin, A.L. (2005). Distinct roles for secreted semaphorin signaling in spinal motor axon guidance. Neuron *48*, 949–964.

Jung, J.M., Choi, J.Y., Kim, H.J., and Seo, W.K. (2015). Statin use in spontaneous intracerebral hemorrhage: a systematic review and meta-analysis. Int. J. Stroke *10* (*Suppl A100*), 10–17.

Kim, W.Y., Gonsiorek, E.A., Barnhart, C., Davare, M.A., Engebose, A.J., Lauridsen, H., Bruun, D., Lesiak, A., Wayman, G., Bucelli, R., et al. (2009). Statins decrease dendritic arborization in rat sympathetic neurons by blocking RhoA activation. J. Neurochem. *108*, 1057–1071.

Koprivica, V., Cho, K.S., Park, J.B., Yiu, G., Atwal, J., Gore, B., Kim, J.A., Lin, E., Tessier-Lavigne, M., Chen, D.F., and He, Z. (2005). EGFR activation mediates inhibition of axon regeneration by myelin and chondroitin sulfate proteoglycans. Science *310*, 106–110.

Lamas, N.J., Johnson-Kerner, B., Roybon, L., Kim, Y.A., Garcia-Diaz, A., Wichterle, H., and Henderson, C.E. (2014). Neurotrophic requirements of human motor neurons defined using amplified and purified stem cell-derived cultures. PLoS ONE *9*, e110324.

Lang, B.T., Wang, J., Filous, A.R., Au, N.P., Ma, C.H., and Shen, Y. (2014). Pleiotropic molecules in axon regeneration and neuroinflammation. Exp. Neurol. *258*, 17–23.

Liu, K., Tedeschi, A., Park, K.K., and He, Z. (2011). Neuronal intrinsic mechanisms of axon regeneration. Annu. Rev. Neurosci. *34*, 131–152.

Ma, T.C., Campana, A., Lange, P.S., Lee, H.H., Banerjee, K., Bryson, J.B., Mahishi, L., Alam, S., Giger, R.J., Barnes, S., et al. (2010). A large-scale chemical screen for regulators of the arginase 1 promoter identifies the soy isoflavone daidzeinas a clinically approved small molecule that can promote neuronal protection or regeneration via a cAMP-independent pathway. J. Neurosci. *30*, 739–748.

Maury, Y., Côme, J., Piskorowski, R.A., Salah-Mohellibi, N., Chevaleyre, V., Peschanski, M., Martinat, C., and Nedelec, S. (2015). Combinatorial analysis of developmental cues efficiently converts human pluripotent stem cells into multiple neuronal subtypes. Nat. Biotechnol. *33*, 89–96.

McTaggart, F., Buckett, L., Davidson, R., Holdgate, G., McCormick, A., Schneck, D., Smith, G., and Warwick, M. (2001). Preclinical and clinical pharmacology of Rosuvastatin, a new 3-hydroxy-3-methylglutaryl coenzyme A reductase inhibitor. Am. J. Cardiol. *87* (*5A*), 28B–32B.

Mukhopadhyay, G., Doherty, P., Walsh, F.S., Crocker, P.R., and Filbin, M.T. (1994). A novel role for myelin-associated glycoprotein as an inhibitor of axonal regeneration. Neuron *13*, 757–767.

Nikulina, E., Tidwell, J.L., Dai, H.N., Bregman, B.S., and Filbin, M.T. (2004). The phosphodiesterase inhibitor rolipram delivered after a spinal cord lesion promotes axonal regeneration and functional recovery. Proc. Natl. Acad. Sci. USA *101*, 8786–8790.

Park, K.K., Liu, K., Hu, Y., Smith, P.D., Wang, C., Cai, B., Xu, B., Connolly, L., Kramvis, I., Sahin, M., and He, Z. (2008). Promoting axon regeneration in the adult CNS by modulation of the PTEN/mTOR pathway. Science *322*, 963–966.

Pihl-Jensen, G., Tsakiri, A., and Frederiksen, J.L. (2015). Statin treatment in multiple sclerosis: a systematic review and meta-analysis. CNS Drugs *29*, 277–291.

Pooler, A.M., Xi, S.C., and Wurtman, R.J. (2006). The 3-hydroxy-3-methylglutaryl co-enzyme A reductase inhibitor pravastatin enhances neurite outgrowth in hippocampal neurons. J. Neurochem. *97*, 716–723.

Posada-Duque, R.A., Velasquez-Carvajal, D., Eckert, G.P., and Cardona-Gomez, G.P. (2013). Atorvastatin requires geranylgeranyl transferase-I and Rac1 activation to exert neuronal protection and induce plasticity. Neurochem. Int. *62*, 433–445.

Qiu, J., Cai, D., Dai, H., McAtee, M., Hoffman, P.N., Bregman, B.S., and Filbin, M.T. (2002). Spinal axon regeneration induced by elevation of cyclic AMP. Neuron *34*, 895–903.

Rabin, S.J., Kim, J.M., Baughn, M., Libby, R.T., Kim, Y.J., Fan, Y., Libby, R.T., La Spada, A., Stone, B., and Ravits, J. (2010). Sporadic ALS has compartment-specific aberrant exon splicing and altered cell-matrix adhesion biology. Hum. Mol. Genet. *19*, 313–328.

Reddy, J.M., Samuel, F.G., McConnell, J.A., Reddy, C.P., Beck, B.W., and Hynds, D.L. (2015). Non-prenylatable, cytosolic Rac1 alters neurite outgrowth while retaining the ability to be activated. Cell. Signal. *27*, 630–637.

Samuel, F., and Hynds, D.L. (2010). RHO GTPase signaling for axon extension: is prenylation important? Mol. Neurobiol. *42*, 133–142.

Saszik, S.M., Robson, J.G., and Frishman, L.J. (2002). The scotopic threshold response of the dark-adapted electroretinogram of the mouse. J. Physiol. *543*, 899–916.

Schulz, J.G., Bösel, J., Stoeckel, M., Megow, D., Dirnagl, U., and Endres, M. (2004). HMG-CoA reductase inhibition causes neurite loss by interfering with geranylgeranylpyrophosphate synthesis. J. Neurochem. *89*, 24–32.

Seelen, M., van Doormaal, P.T., Visser, A.E., Huisman, M.H., Roozekrans, M.H., de Jong, S.W., van der Kooi, A.J., de Visser, M., Voermans, N.C., Veldink, J.H., and van den Berg, L.H. (2014). Prior medical conditions and the risk of amyotrophic lateral sclerosis. J. Neurol. *261*, 1949–1956.

Serajuddin, A.T., Ranadive, S.A., and Mahoney, E.M. (1991). Relative lipophilicities, solubilities, and structure-pharmacological considerations of 3-hydroxy-3-methylglutaryl-coenzyme A (HMG-CoA) reductase inhibitors pravastatin, lovastatin, mevastatin, and simvastatin. J. Pharm. Sci. *80*, 830–834.

Shen, Y., Tenney, A.P., Busch, S.A., Horn, K.P., Cuascut, F.X., Liu, K., He, Z., Silver, J., and Flanagan, J.G. (2009). PTPsigma is a receptor for chondroitin sulfate proteoglycan, an inhibitor of neural regeneration. Science *326*, 592–596.

Skoumbourdis, A.P., Huang, R., Southall, N., Leister, W., Guo, V., Cho, M.H., Inglese, J., Nirenberg, M., Austin, C.P., Xia, M., and Thomas, C.J. (2008). Identification of a potent new chemotype for the selective inhibition of PDE4. Bioorg. Med. Chem. Lett. *18*, 1297–1303.

Snow, D.M., Smith, J.D., Cunningham, A.T., McFarlin, J., and Goshorn, E.C. (2003). Neurite elongation on chondroitin sulfate proteoglycans is characterized by axonal fasciculation. Exp. Neurol. *182*, 310–321.

Thiede-Stan, N.K., and Schwab, M.E. (2015). Attractive and repulsive factors act through multi-subunit receptor complexes to regulate nerve fiber growth. J. Cell Sci. *128*, 2403–2414.

Usher, L.C., Johnstone, A., Ertürk, A., Hu, Y., Strikis, D., Wanner, I.B., Moorman, S., Lee, J.W., Min, J., Ha, H.H., et al. (2010). A chemical screen identifies novel compounds that overcome glial-mediated inhibition of neuronal regeneration. J. Neurosci. *30*, 4693–4706.

van der Most, P.J., Dolga, A.M., Nijholt, I.M., Luiten, P.G., and Eisel, U.L. (2009). Statins: mechanisms of neuroprotection. Prog. Neurobiol. *88*, 64–75.

Wasko, B.M., Smits, J.P., Shull, L.W., Wiemer, D.F., and Hohl, R.J. (2011). A novel bisphosphonate inhibitor of squalene synthase combined with a statin or a nitrogenous bisphosphonate in vitro. J. Lipid Res. *52*, 1957–1964.

Wichterle, H., Lieberam, I., Porter, J.A., and Jessell, T.M. (2002). Directed differentiation of embryonic stem cells into motor neurons. Cell *110*, 385–397.

Yiu, G., and He, Z. (2006). Glial inhibition of CNS axon regeneration. Nat. Rev. Neurosci. *7*, 617–627.

Zhang, F.L., and Casey, P.J. (1996). Protein prenylation: molecular mechanisms and functional consequences. Annu. Rev. Biochem. *65*, 241–269.

Zheng, Z., Sheng, L., and Shang, H. (2013). Statins and amyotrophic lateral sclerosis: a systematic review and meta-analysis. Amyotroph. Lateral Scler. Frontotemporal Degener. *14*, 241–245.

Cell Reports, Volume *16*

Supplemental Information

Protein Prenylation Constitutes an Endogenous Brake on Axonal Growth

Hai Li, Takaaki Kuwajima, Derek Oakley, Elena Nikulina, Jianwei Hou, Wan Seok Yang, Emily Rhodes Lowry, Nuno Jorge Lamas, Mackenzie Weygandt Amoroso, Gist F. Croft, Raghavendra Hosur, Hynek Wichterle, Said Sebti, Marie T. Filbin, Brent Stockwell, and Christopher E. Henderson

Supplementary Experimental Procedures

Neurite outgrowth assay for neuronal cells other than ES-MN

Human ES-MNs, iPS-MNs, Cerebellar granule neurons isolated from postnatal mice (P2 to P6) were plated onto MAG-CHO monolayers grown in 96-well plates similarly to that of ES-MN. After 20 hours, cells were fixed, permeabilized and immunostained with anti-GFP (Invitrogen) or anti-β-III tubulin antibody followed by Alexa Fluor 488 antibody (Invitrogen). The microplates were imaged by Flash Cytometer™ (Trophos) and images were analyzed as described above. Hippocampal neurons (HN) from postnatal day 1 rats were dissociated and purified by OptiPrep gradient centrifugation according to the manufacturer's protocol (Sigma). Purified HNs were resuspended in Sato medium (Doherty et al., 1990), plated onto confluent monolayers of MAG- expressing CHO cells growing in eight-chamber tissue culture slides (Thermo Fisher Scientific, Nunc). Cerivastatin at indicated concentrations were added to the cultures. After 16-18 hours, neurons were fixed and immunostained with anti-β-III tubulin antibody and Alexa Fluor 568 antibody. Images were taken using a Nikon epifluorescence microscope and analyzed with MetaMorph. The numbers represent the average length of the longest neurite of each neuron that was encountered when scanning the slides in a systematic manner (about 600 neurons for each treatment).

Western blot analysis

Confluent monolayers of MAG-expressing CHO cells established in 6-well plate were treated with different concentrations of cerivastatin, simvastatin and blank vehicle for 20-24 hours. Cells were lysed in RIPA buffer (0.1% SDS, 1.0% IGEPAL CA-630, 0.5% sodium deoxycholate, 0.1% SDS, and 50 mM Tris-Cl, pH 8.0) supplemented with protease inhibitors cocktail (Calbiochem). Normalized lysates were subjected to SDS-PAGE, transferred to nitrocellulose membranes, immunostained with a monoclonal antibody to rat MAG (1:1000) (Mukhopadhyay et al., 1994), and incubated overnight at 4°C. After

washes, the membranes were incubated with goat anti-mouse IgG IRDye 680 (Odyssey) for 1 h at room temperature. After washes, membranes were visualized on Odyssey Infrared Imaging System. The blots were re-probed with anti-α-tubulin monoclonal antibody (Sigma) for protein loading control.

Immunohistochemistry

Monolayers of CHO cells were incubated with anti-MAG monoclonal antibody to rat MAG (1:1000 dilution in cold medium, from Dr. Marie Filbin) for 1 hour at 4°C first. Cells were then washed with cold medium three times. After being fixed in 4% PFA for 15 – 30 min at 4°C, cells were blocked with 10% donkey serum in DMEM for 1 hour at room temperature followed by secondary antibody donkey anti-mouse IgG Alexa Fluor 594 (Invitrogen). Images were taken with Nikon epifluorescence microscope using a 4x Apo objective lens at same exposure time for cells treated with different concentrations of statins and control vehicle. The cryosections of optic nerve or retina were washed four times with TBS, blocked with TBS plus 0.5% Triton X-100 plus 1% normal goat serum for 1 h, and then incubated overnight at 4°C with an antibody against growth associated protein-43 (GAP-43; 1:200, Millipore) or β-III tubulin (Tuj1; 1:500, Sigma-Aldrich). The sections were then washed four times with TBS and incubated with a FITC-conjugated goat antibody against rabbit or mouse IgG (1:500, Invitrogen) for 3 h at room temperature. Sections were washed four times and mounted with an aqueous mounting medium before imaging.

SUPPLEMENTARY FIGURES

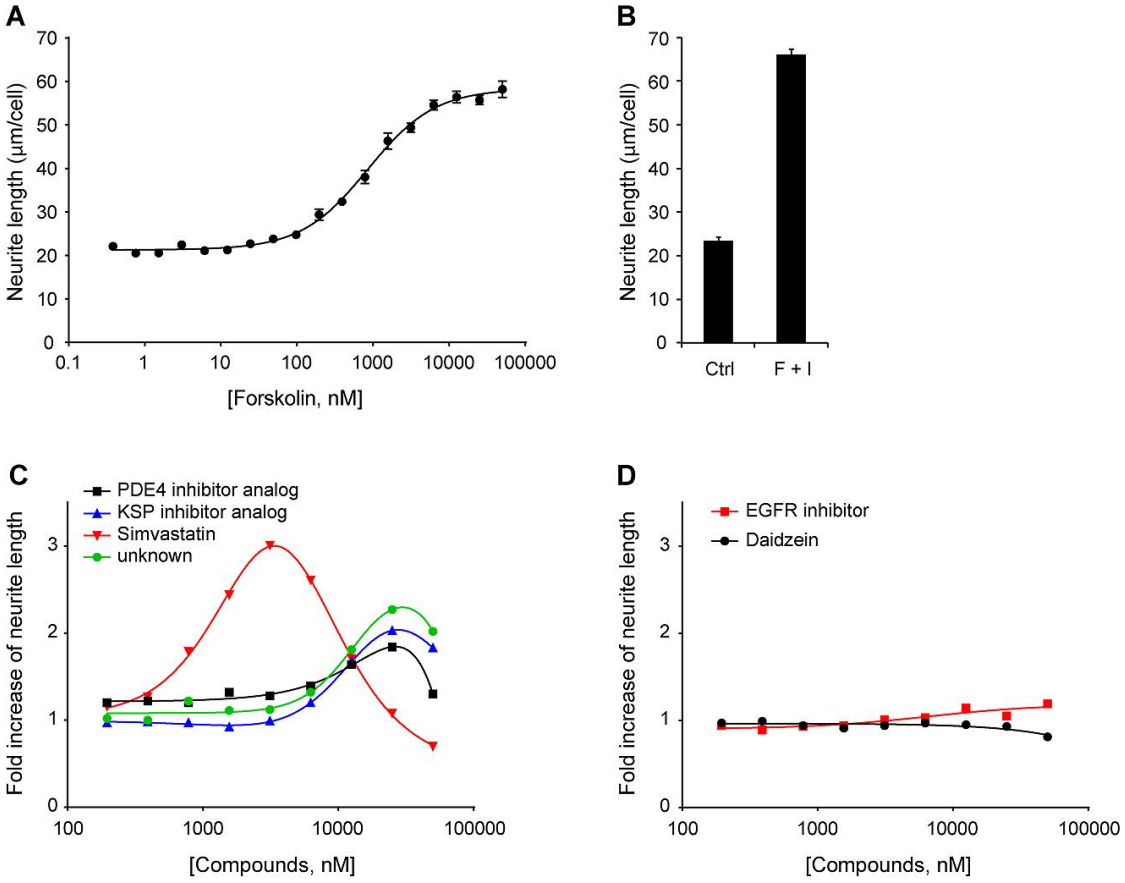

E

Compound	EC_{50} (nM)	IC_{50} (nM)					
	enhanced neurite outgrowth on MAG	inhibit conversion of [^{14}C]acetate into [^{14}C]cholesterol			inhibit HMG-CoA reductase activity *in vitro*	inhibit activity of purified human catalytic domain of HMGCR	inhibit HMGCR activity
	ES-MN	Primary rat hepatocytes	Rat fibroblast cell line NRK-49F	Human umbilical vein endothelial cells HUVECs			Primary rat hepatocytes
Cerivastatin	48.9 ± 0.6	2.5	1.2	3.1	20.8	10	3.54
Fluvastatin	626.6 ± 6.3	4.8	3.4	0.56	44.5	27.6	3.78
Simvastatin	2021.2 ± 3.8	5.2	7.9	1	26.3	11.2	2.74
Mevastatin	2197 ± 10.3				14.1		
Lovastatin	2299.3 ± 10.7				90.9		
Pitavastatin	3640.0 ± 11.1				10.9		
Atorvastatin	9467.0 ± 27.7	0.82	340	5.5	9.1	8.2	1.16
Rosuvastatin	19648.5 ± 122.5	0.3	310	41	40.5	5.4	0.16
Pravastatin	NA	5	14.0 x 10^3	1.9 x 10^3	50.5	44.1	6.93
Forskolin	1006.1 ± 3.4						
Y-27632	18319.6 ± 17.8						

Figure S1. Positive controls and lead compounds identified from the screen, Related to Figure 1

(A) Dose response curve for effect of forskolin on neurite outgrowth over MAG. Note forskolin promotes neurite outgrowth over MAG in dose dependent manner. (B) Neurite outgrowth in vehicle treated cultures (control) vs growth in the presence of the positive control for screening, forskolin 10 μM plus IBMX 100 μM (F+I). (C) Four lead compounds identified from the screen (D) Daidzein and Erthotinib showed no significant activity on neurite outgrowth over MAG-CHO cell monolayer. All data points are mean ± s.e.m.; n=6. Error bars are not shown in (C) and (D) for clarity. (E) Calculated EC_{50} for effect of all 9 statins on neurite outgrowth of ES-MN grown on MAG-CHO (mean ± s.e.m.), and IC_{50} for their inhibitory effect on HMG-CoA reductase activity in various assay system

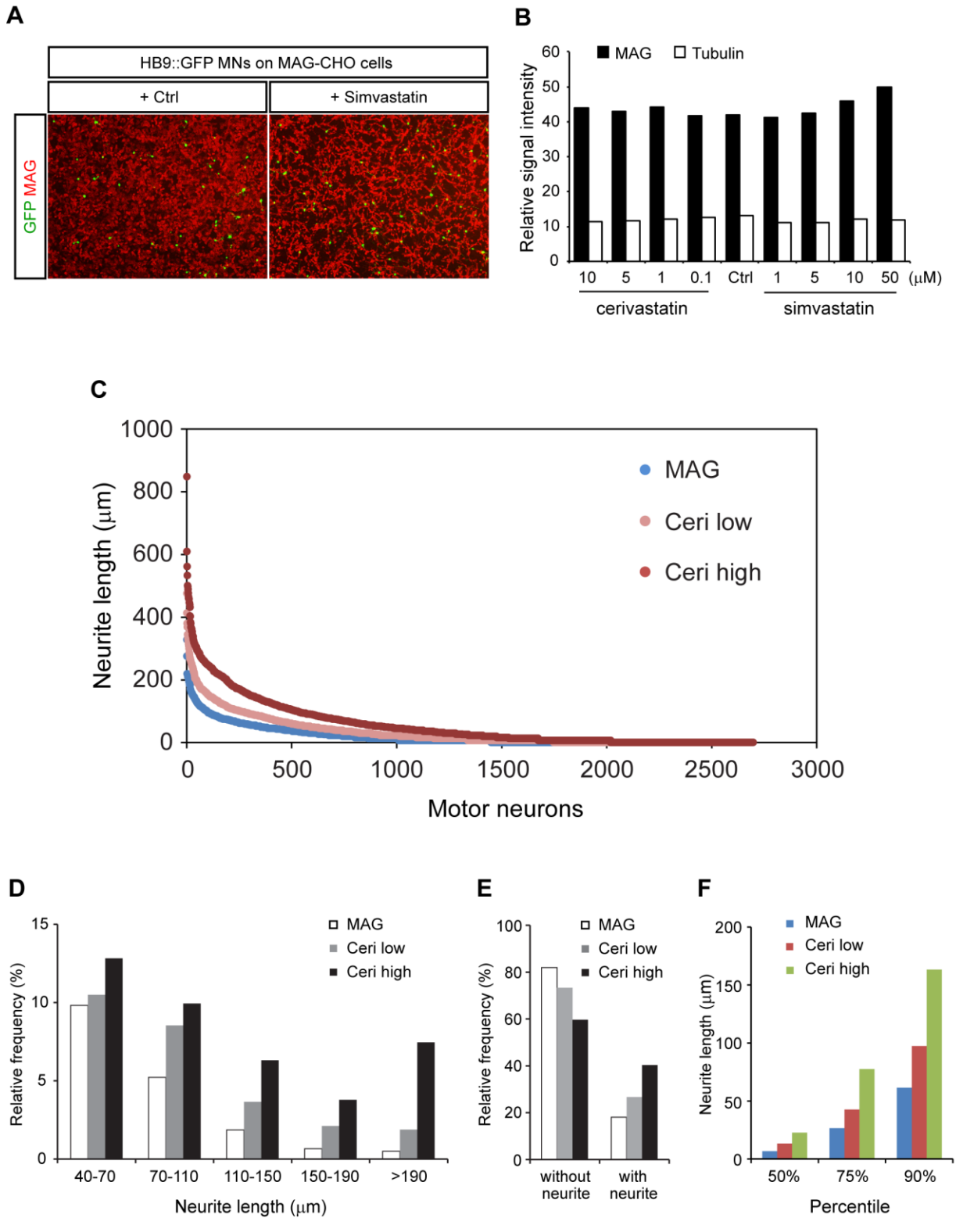
A
HB9::GFP MNs on MAG-CHO cells
+ Ctrl
+ Simvastatin
GFP MAG
B
MAG
Tubulin
Relative signal intensity
60
50
40
30
20
10
0
10
5
1
0.1
Ctrl
1
5
10
50
(μM)
cerivastatin
simvastatin
C
Neurite length (μm)
1000
800
600
400
200
0
0
500
1000
1500
2000
2500
3000
Motor neurons
MAG
Ceri low
Ceri high
D
Relative frequency (%)
15
10
5
0
40-70
70-110
110-150
150-190
>190
Neurite length (μm)
MAG
Ceri low
Ceri high
E
Relative frequency (%)
100
80
60
40
20
0
without neurite
with neurite
MAG
Ceri low
Ceri high
F
Neurite length (μm)
200
150
100
50
0
50%
75%
90%
Percentile
MAG
Ceri low
Ceri high

Figure S2. Statin treatments do not affect MAG protein expression levels in CHO cell monolayer, but increase both neurite initiation and extension in ES-MNs. Related to Figure 2

(A) Immunostaining of MAG protein at surface of CHO cells treated with simvastatin (MAG-CHO cells: red; Hb9::GFP MNs: green). No change was observed in either case. (B) Western blot of MAG protein levels in MAG-CHO cells treated with cerivastatin or simvastatin. Tublin level was used as loading control. (C) Scatter plot for neurite length of all individual ES-MNs grown on MAG-CHO monolayer with vehicle, low (24 nM) and high (391 nM) concentration of cerivastatin. (D) Relative frequency of different length of neurites in response to cerivastatin treatment. Only neurite length above 40 μm are shown here. (E) Percentage of cells without neurites vs. cells with significant neurite length (40 μm above) in cerivastatin and control. (F) Neurite length in 50%, 75% and 90% percentile of all cells in vehicle, low and high concentrations of cerivastatin. Data in (C)-(F) represent cells grown in 6 replicate wells.

A

Inhibitors	EC_{50} for axon regeneration (μM)	IC_{50} for FTase (μM)	IC_{50} for GGTase (μM)	Reference
GGTI-298	2.6 ± 0.2	>15 *	3 **	Qian et al., 1998
FTI-277	5.6 ± 0.3	0.1 *	>10 **	Lerner et al., 1995
GGTI-2417	10.6	>50 *	0.4 **	Kazi et al., 2009
FTI-2153	0.21	0.01 *	>30 **	Sun et al., 1999

* Farnesylation of H-Ras

** Geranylgeranylation of Rap1A

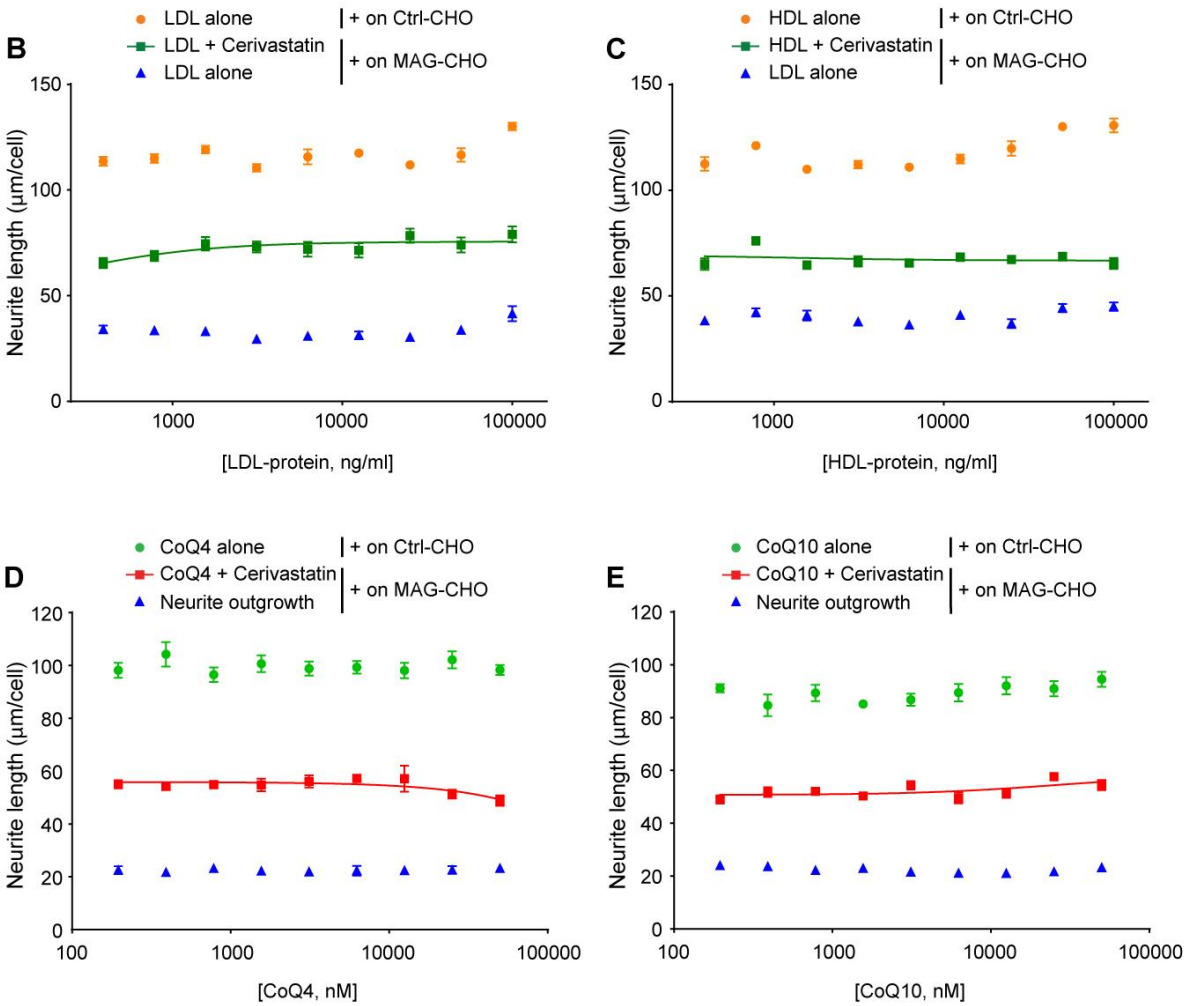

Figure S3. Statins promote neurite growth by inhibiting protein prenylations, not by inhibiting synthesis of cholesterol and isoprenoids. Related to Figure 3

(A) Calculated EC50 for effect of GGTIs and FTIs on neurite outgrowth over MAG inhibition, and their published IC50 for inhibiting protein prenylation. Effect of (B) LDL-proteins, (C) HDL-proteins, (D) Isoprenoid CoQ4 and (E) CoQ10 on neurite outgrowth over control CHO, MAG-CHO with and without promotional effect of cerivastatin.

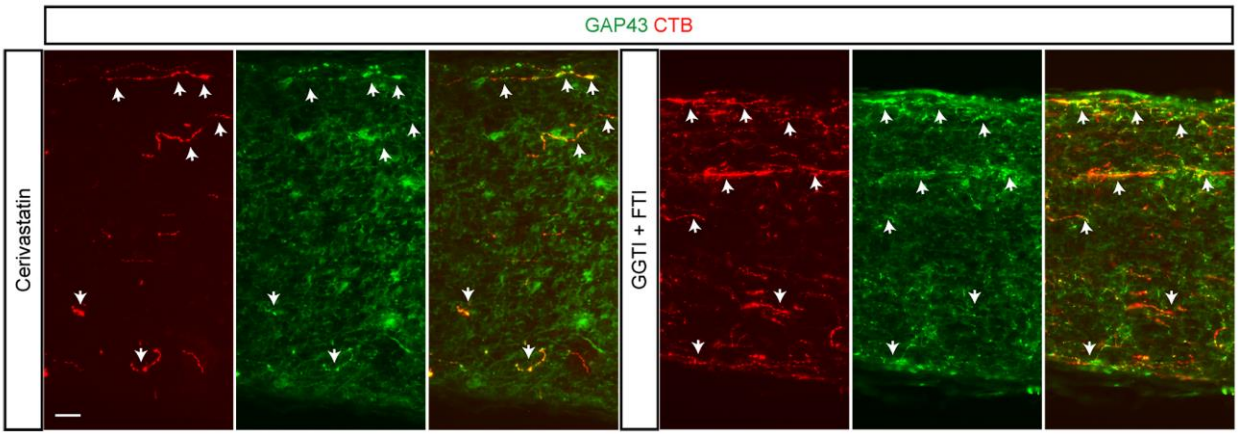

Figure S4. Regrowing axons by cerivastatin or prenylation inhibitors in injured optic nerve highly express GAP43. Related to Figure 4

GAP43, a maker of regenerating axons is highly expressed on CTB-labeled regrowing retinal axons in cerivastatin or combinations of GGTI and FTI (GGTI + FTI)-treated mice (arrows). Scale bar, 20 μm.

References

DOHERTY, P., COHEN, J. & WALSH, F. S. 1990. Neurite outgrowth in response to transfected N-CAM changes during development and is modulated by polysialic acid. *Neuron,* 5, 209-19.

KAZI, A., CARIE, A., BLASKOVICH, M. A., BUCHER, C., THAI, V., MOULDER, S., PENG, H., CARRICO, D., PUSATERI, E., PLEDGER, W. J., BERNDT, N., HAMILTON, A. & SEBTI, S. M. 2009. Blockade of protein geranylgeranylation inhibits Cdk2-dependent p27Kip1 phosphorylation on Thr187 and accumulates p27Kip1 in the nucleus: implications for breast cancer therapy. *Molecular and cellular biology,* 29, 2254-63.

LERNER, E. C., QIAN, Y., BLASKOVICH, M. A., FOSSUM, R. D., VOGT, A., SUN, J., COX, A. D., DER, C. J., HAMILTON, A. D. & SEBTI, S. M. 1995. Ras CAAX peptidomimetic FTI-277 selectively blocks oncogenic Ras signaling by inducing cytoplasmic accumulation of inactive Ras-Raf complexes. *The Journal of biological chemistry,* 270, 26802-6.

MUKHOPADHYAY, G., DOHERTY, P., WALSH, F. S., CROCKER, P. R. & FILBIN, M. T. 1994. A novel role for myelin-associated glycoprotein as an inhibitor of axonal regeneration. *Neuron,* 13, 757-67.

QIAN, Y., VOGT, A., VASUDEVAN, A., SEBTI, S. M. & HAMILTON, A. D. 1998. Selective inhibition of type-I geranylgeranyltransferase in vitro and in whole cells by CAAL peptidomimetics. *Bioorganic & medicinal chemistry,* 6, 293-9.

SUN, J., BLASKOVICH, M. A., KNOWLES, D., QIAN, Y., OHKANDA, J., BAILEY, R. D., HAMILTON, A. D. & SEBTI, S. M. 1999. Antitumor efficacy of a novel class of non-

thiol-containing peptidomimetic inhibitors of farnesyltransferase and geranylgeranyltransferase I: combination therapy with the cytotoxic agents cisplatin, Taxol, and gemcitabine. *Cancer research*, 59, 4919-26.